

---

Theses and Dissertations

---

Spring 2015

# Formation of haloacetic acids and N-nitrosodimethylamine via the chlorination of carbon nanotubes

Kyle Jeffery Nelson  
*University of Iowa*

Copyright 2015 Kyle Nelson

This thesis is available at Iowa Research Online: <https://ir.uiowa.edu/etd/1708>

---

## Recommended Citation

Nelson, Kyle Jeffery. "Formation of haloacetic acids and N-nitrosodimethylamine via the chlorination of carbon nanotubes." MS (Master of Science) thesis, University of Iowa, 2015.  
<https://doi.org/10.17077/etd.igro9blf>.

---

Follow this and additional works at: <https://ir.uiowa.edu/etd>

 Part of the [Civil and Environmental Engineering Commons](#)

FORMATION OF HALOACETIC ACIDS AND N-NITROSODIMETHYLAMINE VIA  
THE CHLORINATION OF CARBON NANOTUBES

by  
Kyle Jeffery Nelson

A thesis submitted in partial fulfillment  
of the requirements for the Master of  
Science degree in Civil and Environmental Engineering  
in the Graduate College of  
The University of Iowa

May 2015

Thesis Supervisor: Associate Professor David M. Cwiertny

Thesis Co-Advisor: Professor Richard L. Valentine

Copyright by  
KYLE JEFFERY NELSON  
2015  
All Rights Reserved

Graduate College  
The University of Iowa  
Iowa City, Iowa

CERTIFICATE OF APPROVAL

---

MASTER'S THESIS

---

This is to certify that the Master's thesis of

Kyle Jeffery Nelson

has been approved by the Examining Committee  
for the thesis requirement for the Master of Science  
degree in Civil and Environmental Engineering at the May 2015 graduation.

Thesis Committee: \_\_\_\_\_  
David M. Cwiertny, Thesis Supervisor

\_\_\_\_\_  
Richard L. Valentine, Thesis Co-Advisor

\_\_\_\_\_  
Timothy E. Mattes

## ACKNOWLEDGMENTS

Firstly, I would like to thank both of my graduate advisors, Dr. David Cwiertny and Dr. Richard Valentine. Dave, thank you for all of your guidance over these last six years. You have truly made a huge impact on my life and career, and I cannot thank you enough for this opportunity. Rich, thank you for your constant encouragement and for sharing with me your vast amount of knowledge. Through all of the ups and downs, you two helped make this experience one of the most rewarding tasks I have accomplished.

I would also like to thank everyone in the Cwiertny group and Environmental Engineering department at the University of Iowa. You all have made this journey much more feasible and become great friends along the way.

Thank you to Edgard Verdugo for all of his support on this project. I am forever thankful for his willingness to always assist me in my experiments and data analysis.

I also have to thank my family and friends back home for all of their love and support throughout this adventure – especially my Mom, Dad, and Emily for their involvement in my life and for providing me with a loving, caring environment.

I especially want to thank my fiancée, Allison, for all of her love and support on our journey together. She has been my backbone and has helped me keep my head above the water, even when times were tough. I love you.

Lastly, I want to thank God for giving me the patience and strength to succeed in graduate school. I would not have been able to make it through without His love.

## ABSTRACT

Recent investigations have shown that engineered nanomaterials such as carbon nanotubes (CNTs) are a source and precursor for disinfection byproduct (DBP) formation. The aim of this study was to extend previous research of CNTs by investigating the potential for other classes of CNTs to generate disinfection byproducts (DBP) during chlorination. We examined particular types of CNTs with surface groups analogous to suspected model precursors for DBP formation. Specifically, we conducted experiments to determine the formation of haloacetic acids (HAAs) and N-nitrosodimethylamine (NDMA) via the chlorination of carbon nanotubes.

Polymer coated CNTs generated the greatest total HAA concentration of up to 170  $\mu\text{g-HAA/mg-CNT}$ . Results showed that the presence of surface oxide groups (e.g. surface carboxylic acid groups) promotes HAA formation. We observed a strong correlation between the extent of HAA formation and the concentration of surface oxygen on the CNT surface. Results also showed that CNTs behave similar to model precursors for di- and trichloroacetic acid formation (DCAA and TCAA, respectively).

Nitrogen containing CNTs have been shown as source of N-nitrosodimethylamine (NDMA). Surprisingly, polyethylene glycol functionalized CNTs, which does not contain N, produces NDMA when reacted with chlorine and ethylenediamine (EDA). Ultimately, EDA is contributing N to CS PEG by sorbing to the CNT surface, which is the likely source of N for NDMA formation. At lower EDA concentrations, NDMA production is limited by available EDA. Conversely, at higher EDA concentrations, NDMA production is limited by available chlorine that is in competition with EDA and the CNT surface.

## PUBLIC ABSTRACT

Chlorination of drinking water is commonly used due to the capability of disinfection (microorganisms inactivation) and oxidation (taste and odor control). Even though disinfectants are efficient at removing target pollutants, due to the strong oxidation potential and relatively limited selectivity, a shortcoming is that disinfectants can react with non-specific compounds to generate harmful by-products. Most commonly during treatment disinfectants react with natural organic matter (NOM) or other soluble organic substances to form disinfection byproducts (DBPs).

Recent investigations have shown that engineered nanomaterials such as carbon nanotubes (CNTs) are a source and precursor for DBP formation. The aim of this study was to extend previous research of CNTs by investigating the potential for other classes of CNTs to generate disinfection byproducts (DBP) during chlorination. We examined particular types of CNTs with surface groups analogous to suspected model precursors for DBP formation. Specifically, we conducted experiments to determine the formation of haloacetic acids (HAAs) and N-nitrosodimethylamine (NDMA) via the chlorination of carbon nanotubes.

Our work has shown that there is a strong correlation between the surface oxygen content on CNTs and the formation potential of HAAs. Additionally, a novel pathway for NDMA production was observed when non N-containing CNTs were chlorinated in the presence of a nitrogen containing compound.

## TABLE OF CONTENTS

LIST OF TABLES.....	vii	
LIST OF FIGURES.....	viii	
CHAPTER 1 INTRODUCTION		
1.1 Disinfection Practices .....	1	
1.2 Disinfection Byproducts .....	4	
1.3 Disinfection Byproduct Formation, Sources, and Precursors.....	7	
1.4 Carbon Nanotubes as Next Generation Precursors.....	12	
1.5 Overall Objective, Hypothesis, and Specific Aims .....	14	
CHAPTER 2 MATERIALS AND METHODS .....		15
2.1 Reagents.....	15	
2.2 Carbon Nanotubes .....	16	
2.3 General Procedures.....	18	
2.3.1 Haloacetic Acid Formation Experiments .....	18	
2.3.2 N-Nitrosodimethylamine Formation Experiments .....	19	
2.3.3 Ethylenediamine Sorption Experiments .....	20	
2.4 Analytical Methods.....	20	
2.4.1 HOCl Titrations .....	20	
2.4.2 Haloacetic Acid Analysis .....	21	
2.4.3 N-Nitrosodimethylamine Analysis .....	22	
2.4.4 Ehtylenediamine Analysis .....	23	
CHAPTER 3 HALOACETIC ACID FOMRATION DURING CHLORINATION OF CARBON NANOTUBES .....		24
3.1 Introduction.....	24	
3.2 HAA Production during Chlorination of Various Carbon Nanotube Formulations.....	26	
3.3 Influence of Experimental Parameters on HAA Formation .....	30	
3.4 HAA Formation Kinetics.....	35	
3.5 Oxidation State of Carbon Nanotubes .....	40	
3.6 Environmental Implications.....	46	
CHAPTER 4 N-NITROSODIMETHYLAMINE PRODUCTION DURING THE CHLORINATION OF CARBON NANOTUBES .....		48
4.1 Introduction.....	48	
4.2 NDMA Formation via the Reaction of Carbon Nanotubes, Chlorine, and Ethylenediamine .....	50	
4.3 EDA Sorption .....	54	
4.4 Experimental Variables Influencing NDMA Formation in CS PEG Suspensions .....	56	
4.5 Effect of Chlorine Dose.....	59	
4.6 Conclusions.....	61	

CHAPTER 5 ENVIRONMENTAL IMPLICATIONS AND FUTURE WORK.....	63
5.1 Environmental Implications.....	63
5.2 Future Work.....	64
REFERENCES.....	65

## LIST OF TABLES

Table 1.1. Regulated and emerging DBP classes. ....	6
Table 2.1. List of functionalities of purchased CNTs. Non-functionalized CNTs are not shown. ....	16
Table 3.1. MCAA, DCAA, TCAA, and total HAA formation in $\mu\text{g-HAA/mg-CNT}$ and the corresponding chlorine consumption. CNTs that did not produce detectable limits of HAAs are listed as ND. CNTs that did produce HAAs, but were not quantifiable are listed as NQ. Chloroform (CF) data were provided by Verdugo [62]. Experiments were conducted in the same conditions as Figure 3.1. ....	28
Table 4.1. N-CNTs utilized in the Verdugo study. ....	48
Table 4.2. NDMA formation from commercial non N-CNTs and CS PABS at 10 mg/L when reacted with 15 mg/L HOCl and 1000 $\mu\text{g/L}$ EDA. *CS PABS produced NDMA with and without the presence of EDA. ....	51

## LIST OF FIGURES

Figure 1.1. Effect of pH on chlorine speciation. Adapted from Deborde [1] .....	2
Figure 1.2. Chlorine equilibria in solution at 25 °C. Adapted from Doré [4]. .....	2
Figure 1.3. Primary reaction of ozone with a compound S. Adapted from von Gunten [6]. .....	3
Figure 1.4. UV light disinfection at 254 nm wavelength. Adapted from Radiant UV [9].	4
Figure 1.5. Compounds commonly used as model precursors for carbonaceous (C-DBP) and nitrogenous (N-DBP) disinfection byproducts. ....	10
Figure 2.1. Schematic of CS PEG functionalization route. Adapted from Zhao <i>et al</i> [57]. .....	18
Figure 3.1. Fraction of initial chlorine consumed after 4 h of reaction for all CNTs considered herein. Experiments were conducted in 5 mM phosphate buffer of 10 mg/L CNT loading and 15 mg/L HOCl dose. ....	27
Figure 3.2. MCAA formation for varied CNT loadings of 5, 10, and 20 mg/L. Experiments were conducted in 5 mM phosphate buffer with 15 mg/L HOCl, and reacted for 4 hours. The upper figure shows non-functionalized, nitrogenated, and carboxylated CNTs, while the lower figure shows the polymer functionalized CNTs. ....	31
Figure 3.3. DCAA formation for varied CNT loadings of 5, 10, and 20 mg/L. Experiments were conducted in 5 mM phosphate buffer with 15 mg/L HOCl, and reacted for 4 hours. The upper figure shows non-functionalized, nitrogenated, and carboxylated CNTs, while the lower figure shows the polymer functionalized CNTs. ....	32

Figure 3.4. TCAA formation for varied CNT loadings of 5, 10, and 20 mg/L.  
 Experiments were conducted in 5 mM phosphate buffer with 15 mg/L HOCl, and reacted for 4 hours. The upper figure shows non-functionalized, nitrogenated, and carboxylated CNTs, while the lower figure shows the polymer functionalized CNTs. .... 33

Figure 3.5. Chlorine decay kinetics for CS PABS, CS SWCOOH, and CS SWNF.  
 Experiments conducted at pH 8 5 mM phosphate buffer with 10 mg/L CNT loading and 15 mg/L HOCl. Samples were taken at 1, 2, 4, 7, 11, 24, and 48 h. .... 36

Figure 3.6. HAA formation kinetics for CS SWCOOH. Experiments conducted at pH 8 5 mM phosphate buffer with 10 mg/L CNT loading and 15 mg/L HOCl. Samples were taken at 1, 2, 4, 7, 11, 24, and 48 h. .... 37

Figure 3.7. HAA formation kinetics for CS PABS. Experiments conducted at pH 8 5 mM phosphate buffer with 10 mg/L CNT loading and 15 mg/L HOCl. Samples were taken at 1, 2, 4, 7, 11, 24, and 48 h. .... 37

Figure 3.8. HAA formation per chlorine consumed as a function of time for CS PABS and CS SWCOOH. .... 40

Figure 3.9. (a) Total HAA, (b) MCAA, (c) DCAA, and (d) TCAA formation per CNT loading as a function of surface oxygen content as measured by the O 1s region from XPS. All figures are on the same y-axis for comparison between different HAA classes. .... 42

Figure 3.10. Fraction of initial chlorine consumed after reacted with chlorine for 4 h. Experiments were conducted in 5 mM phosphate buffer of 10 mg/L CNT loading and 15 mg/L HOCl dose. ....	45
Figure 3.11. Mechanism of TCAA and chloroform formation via the chlorination of resorcinol.....	46
Figure 4.1. (a) NDMA formation and (b) normalized chlorine consumption during chlorination of CS PEG suspension. Experiments were conducted at pH 8 in 5 mM phosphate buffer with 10 mg/L CS PEG CNT loading, 15 mg/L HOCl, and 2000 µg/L EDA. ....	53
Figure 4.2. EDA sorption per CNT loading as a function of EDA remaining in solution. Experiments were conducted at pH 8 in 5 mM phosphate buffer with 10 mg/L of CS PEG, NL SWCOOH, and NL SWNF and reacted with varied EDA concentrations (200 - 5000 µg/L) for 1 day. ....	56
Figure 4.3. (a) NDMA formation and (b) fraction of initial chlorine consumed as a function of varied EDA added for varied CS PEG loadings. Experiments were conducted at pH 8 in 5 mM phosphate buffer with 15 mg/L of HOCl reacted for 1 day. ....	57
Figure 4.4. (a) NDMA formation and (b) fraction of initial chlorine consumed as a function of EDA added for varied HOCl doses. Experiments were conducted at pH 8 in 5 mM phosphate buffer with a fixed loading of CS PEG (10 mg/L) and reacted for 1 day. ....	60

## CHAPTER 1 INTRODUCTION

### 1.1 Disinfection Practices

Disinfection of treated waters is an effective strategy for the inactivation of waterborne pathogens including bacteria, viruses, and amoebic cysts. Common disinfectants used in drinking water treatment include free chlorine (HOCl) and combined chlorine (e.g., chloramines), ozone, and ultraviolet (UV) radiation. Due to their strong oxidative nature, these disinfectants exhibit high reactivity toward these target microorganisms, with some being more effective than others [1]. This high reactivity is most desirable to ensure effective destruction or inactivation of disease-causing organisms and best achieve the stringent regulations enforced for pathogen removal (e.g., the US EPA requires 99.9% inactivation of *Giardia lamblia* cysts during drinking water treatment). Preferably, disinfectants performance should be invariant across various source water compositions. Further, they must also be cost effective and not pose a human health risk at the levels needed to produce sufficient residual protection against possible contamination in the distribution system [2].

Due to its low cost, chlorine is the most widely used disinfectant. Forms of chlorine most commonly employed during water treatment include gaseous chlorine ( $\text{Cl}_2$ ) and sodium hypochlorite ( $\text{NaOCl}$ ) [1]. In natural waters between pH 6-9, hypochlorous acid (HOCl) and hypochlorite ( $\text{ClO}^-$ ) are the dominant chlorine species (see Figure 1.1). The more reactive form is HOCl, which predominates at pH values below the  $\text{pK}_a = 7.5$  for its dissociation to  $\text{ClO}^-$  (see Figure 1.2). Thus, the efficiency of chlorine as a disinfectant is highly pH dependent, with performance generally decreasing with

increasing pH as total chlorine speciation shifts to favor hypochlorite over hypochlorous acid. Other species of chlorine are typically too low in concentration or show insufficient reactivity to be significant in natural waters [3].

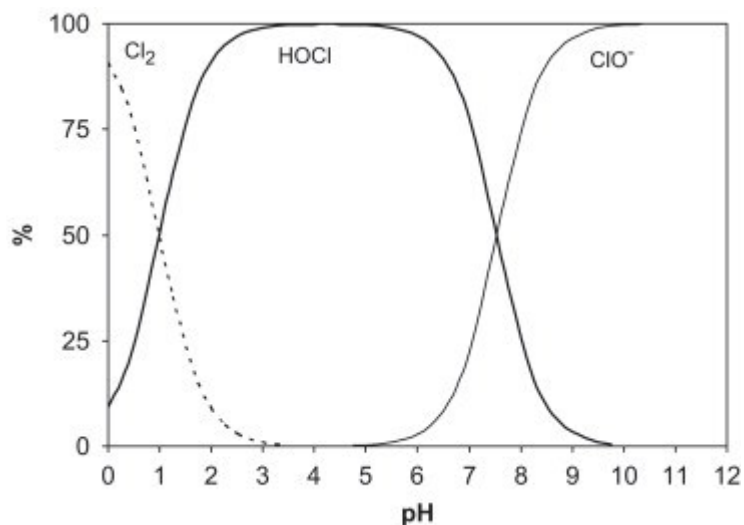
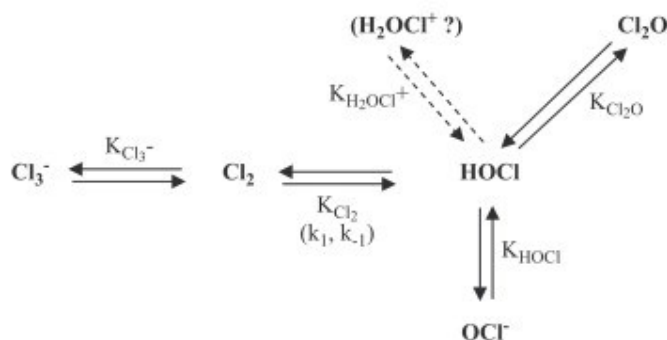


**Figure 1.1.** Effect of pH on chlorine speciation. Adapted from Deborde [1]



Equations	equilibrium constants (25°C)	references
$\text{HOCl} \rightleftharpoons \text{ClO}^- + \text{H}^+$	$K_{\text{HOCl}} = 2.9 \times 10^{-8}$	(Morris, 1966)
$\text{Cl}_2 + \text{H}_2\text{O} \rightleftharpoons \text{HOCl} + \text{H}^+ + \text{Cl}^-$	$K_{\text{Cl}_2} = 5.1 \times 10^{-4} \text{ M}^2$ ( $k_1 = 22.3 \text{ s}^{-1}$ , $k_{-1} = 4.3 \times 10^4 \text{ M}^{-2} \text{ s}^{-1}$ )	(Wang and Margerum, 1994)
$\text{H}_2\text{OCl}^+ \rightleftharpoons \text{HOCl} + \text{H}^+$	$K_{\text{H}_2\text{OCl}^+} = 10^{-3} - 10^{-4}$	(Arotsky and Symons, 1962)
$2 \text{HOCl} \rightleftharpoons \text{Cl}_2\text{O} + \text{H}_2\text{O}$	$K_{\text{Cl}_2\text{O}} = 8.7 \times 10^{-3}$	(Reinhard and Stumm, 1980)
$\text{Cl}_2 + \text{Cl}^- \rightleftharpoons \text{Cl}_3^-$	$K_{\text{Cl}_3^-} = 0.191$	(Zimmermann and Strong, 1957)

**Figure 1.2.** Chlorine equilibria in solution at 25 °C. Adapted from Doré [4].

Chloramines are formed from the reaction of hypochlorous acid and ammonium. This oxidation results from successive reactions which firstly induce chloramine (mono-, di-, and tri-chloramines) formation [1]. The distribution of types of chloramines is dependent on the pH, temperature, time, and initial chlorine to ammonium ratio. Chloramines possess similar oxidative properties as free chlorine but varies with pH [2].

Aside from chlorine-based disinfectants, ozone and UV radiation are alternative disinfection options to overcome some of the disadvantages of chlorine. In ozone reactions, there are two ways of oxidation: direct reaction between ozone and dissolved compounds, and the reaction between hydroxyl radicals and dissolved compounds. Ozone is effective over a wide pH range and has a stronger oxidizing power within a shorter reaction time as compared to chlorination [5].

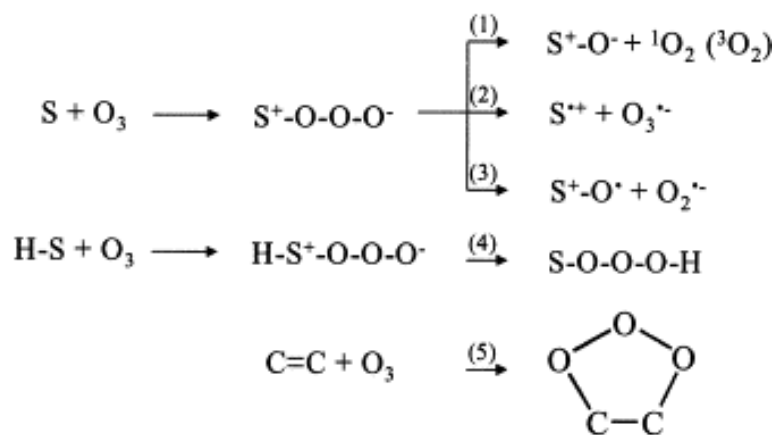


**Figure 1.3.** Primary reaction of ozone with a compound S. Adapted from von Gunten [6].

UV radiation is generated by the flow of electrons from an electrical source through ionized mercury vapor in a lamp [2]. In water treatment systems, UV light is transmitted in the UVC range which is a wavelength between 200-280 nm. At these wavelengths, there is enough energy to cause modifications or actual breaks in DNA [7]. This provides optimum conditions for inactivation of microorganisms in the treated water

[8]. Figure 1.4 shows how UV light sterilizes microorganisms via the photochemical destruction of DNA [9].

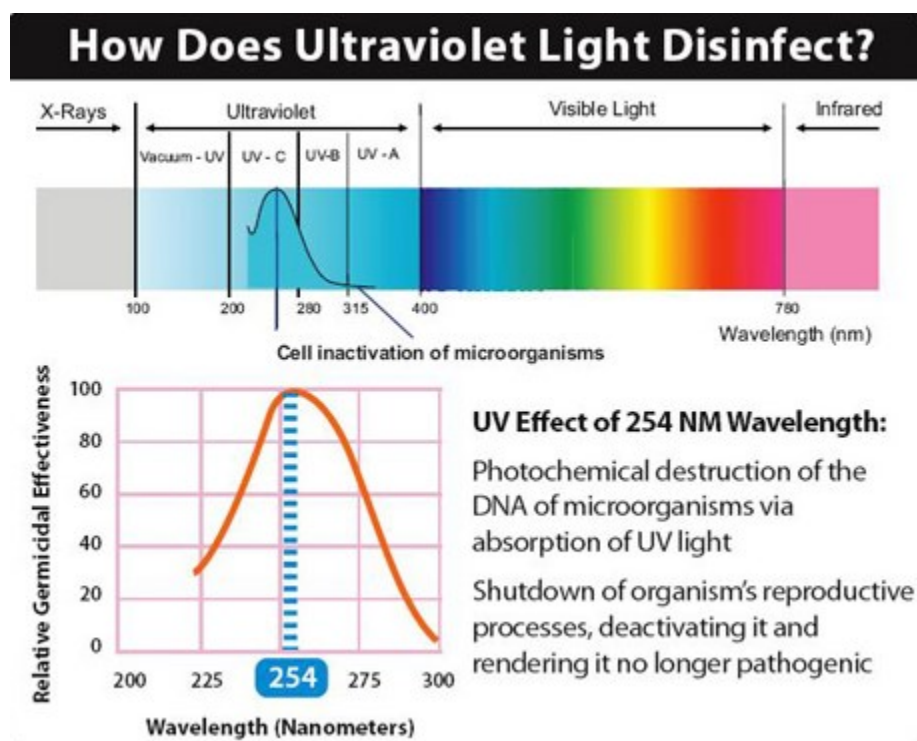


**Figure 1.4.** UV light disinfection at 254 nm wavelength. Adapted from Radiant UV [9].

### 1.2 Disinfection Byproducts

Several studies have been done to model the reaction of chlorine in the presence of organic or inorganic compounds [10-12]. Most chlorine reactions with these compounds are second order in oxidation kinetics. Hypochlorous acid is the most dominant reactive species of chlorine with the majority of organic compounds. Due to the oxidizing power and chemical bond, HOCl can react three different ways with organic compounds[1]. Thus, this disinfectant provides the highest selectivity towards organic micropollutants.

Even though disinfectants are efficient at removing target pollutants, due to the strong oxidation potential and relatively limited selectivity, a shortcoming is that

disinfectants can react with non-specific compounds to generate harmful by-products. Most commonly during treatment disinfectants react with natural organic matter (NOM) or other soluble organic substances to form disinfection byproducts (DBPs). To date, over 600 types of DBPs have been identified for drinking water disinfectants [13]. DBPs are broadly classified as either halogenated or non-halogenated, and can be further broken down to carbonaceous (C-DBPs) or nitrogenous (N-DBPs) byproducts. Table 1.1 lists selected DBPs that are “high priority” for future regulatory action.

Halogenated byproducts containing chlorine (from HOCl), as well as bromine and/or iodine when Br<sup>-</sup> and I<sup>-</sup> are present in the water supply, are the most common DBPs in drinking waters. In 1988, a study found that halogenated DBPs accounted for 30 – 60% of total organic halogens in drinking water [14]. On a weight basis, trihalomethanes (THMs) and haloacetic acids (HAAs) are the largest class of DBPs [15]. Due to their potential risks to human health, THMs and HAAs are regulated under the United States Environmental Protection Agency’s Disinfectant and Disinfection Byproducts (D/DBP) rule. Total trihalomethanes, which includes bromodichloromethane, bromoform, dibromochloromethane, and chloroform, have a US EPA enforceable maximum contaminant level (MCL) of 80 µg/L. The sum of five HAAs, monochloroacetic acid, dichloroacetic acid, trichloroacetic acid, bromoacetic acid, and dibromoacetic acid (also referred to as HAA5), has an MCL of 60 µg/L as an annual average. People who have consumed water containing THMs could experience liver, kidney, or central nervous problems and may have an increased risk of cancer, while HAAs can lead to increased incidents of cancer, as well as reproductive and developmental effects [16].

Table 1.1. Regulated and emerging DBP classes.

Category	Species	Structure
Trihalomethanes (THM4)	Chloroform	
	Bromoform	
	Dichlorobromomethane	
	Dibromochloromethane	
Haloacetic Acids (HAA5)	Monochloroacetic Acid (MCAA)	
	Monobromoacetic Acid (MBAA)	
	Dichloroacetic Acid (DCAA)	
	Dibromoacetic Acid (DBAA)	
	Trichloroacetic Acid (TCAA)	
Nitrosoamines	N-nitrosodimethylamine (NDMA)	
	N-nitrosomethylamine (NMEA)	
	N-nitrosodiethylamine (NDEA)	
	N-nitroso-di-n-propylamine (NDPA)	
	N-nitroso-di-n-butylamine (NDPA)	
	N-nitroso-di-phenylamine (NDPhA)	
	N-nitrosopyrrolidine (NPIP)	
N-nitrosopiperidine (NPIP)		
Halonitromethanes (HNMs)	Chloronitromethane (CNM)	
	Bromonitromethane (BNM)	
	Bromodichloronitromethane (BDCNM)	
	Dibromochloronitromethane (DBCNM)	
	Trichloronitromethane (TCNM)	
	Dichloronitromethane (DCNM)	
Haloacetonitriles (HANs)	Chloroacetonitrile (MCAN)	
	Bromoacetonitrile (MBAN)	
	Dichloroacetonitrile (DCAN)	
	Dibromoacetonitrile (DBAN)	
	Bromochloroacetonitrile (BCAN)	
	Trichloroacetonitrile (TCAN)	
Iodo/bromo acetic acid	Iodoacetic Acid (IAA)	
	Bromoacetic Acid (BAA)	
Iodo methanes	Iodoform	

Perhaps the most significant class of non-halogenated DBP is nitrosoamines, which are N-DBPs. Nitrosoamines are primarily formed from the reaction of monochloramine with substances containing organic nitrogen. One particular nitrosamine of concern is *N*-Nitrosodimethylamine (NDMA), which has been identified by the EPA as an extremely potent human carcinogen [17]. Typically, nitrosoamines occur at lower concentrations in drinking waters compared to THMs and HAAs. Even so, the cancer potency of NDMA is much higher than that of trihalomethanes [18]. In fact, nitrosamines are one of five groups of DBPs (in addition to iodinated DBPs, halonitromethanes, and halonitriles) that have been identified as high priority emerging contaminant classes [18] because of their high cell cytotoxicity and genotoxicity of mammalian cells [19, 20]. Likely, rising concern over their human health risks will drive these DBPs to be regulated in the next couple of years. However, to date, NDMA does not have a MCL set for drinking water, although the USEPA has determined that its maximum admissible concentration in drinking water is 7 ng/L (ppt). California has established a non-enforceable Public Health Goal of 3 ng/L.

### 1.3 Disinfection Byproduct Formation, Sources, and Precursors

Numerous studies have investigated the role of NOM and other forms of dissolved organic carbon as precursors to DBPs including trihalomethanes, haloacetic acids, and nitrosoamines. Despite this extensive body of literature, a detailed mechanism for DBP formation has not yet been established, in part due to the complexity of NOM. The composition of NOM, which is composed of humic substances, carboxylic acids, amino acids, proteins, and carbohydrates [21], is known to influence DBP formation. An excellent predictor of the aromatic content of NOM is the specific ultraviolet absorbance

(SUVA), which is the ratio between the ultraviolet absorbance measured at 254 nm (UV<sub>254</sub>) and the dissolved organic carbon (DOC) content [22, 23]. For example, work by Liang and Singer revealed that NOM precursors with higher SUVA values produced more haloacetic acids [24]. For example, it has been shown that halogenated DBPs increase as the aromatic content of NOM increases [25].

NOM can also be divided into hydrophobic or hydrophilic fractions [26], and these organic fractions can be further subdivided into six categories: hydrophobic acids (HPOA), hydrophobic bases (HPOB), hydrophobic neutrals (HPON), hydrophilic acids (HPIA), hydrophilic bases (HPIB), and hydrophilic neutrals (HPIN). Kanokkantapong *et al.* [22] successfully characterized the prominent functional groups of these fractions, with the hydrophobic fractions typically being heavier in molecular weight. For these hydrophobic fractions (HPOA, HPOB, and HPON) target functional groups contributing to HAA formation were carboxylic acids, amide and amino acids, and ketone, respectively. More generally, studies have also shown that the distribution of hydrophobic and hydrophilic fractions influences the relative extent of THM and HAA formation, with hydrophobic precursors more generally favoring HAA production than THMs [24, 27].

The formation of DBPs is largely dependent on the source water quality characteristics. The concentration and nature of organic precursors, water temperature, pH, and disinfectant dose, contact time, and point of addition are the most important parameters in influencing the formation potential of DBPs [24]. Of these, the chlorination pH has been shown to greatly affect the type of DBP that is prevalent in drinking water. Liang *et al.* [24] showed that increasing the pH from 6 to 8 increased the formation of

THMs, but significantly decreased the formation of DCAA and TCAA. MCAA did not experience any change in concentration across this pH range. The effect of pH on HAA concentrations is likely due to the reaction mechanisms proposed by Reckhow and Singler [25]; in more acidic environments, the R group of the common precursor structure (R-CO-CX<sub>3</sub>) is readily oxidized to donate an electron pair for DCAA and TCAA formation.

Given the complexity of NOM, a more simplified picture of DBP formation mechanisms is often achieved using lower molecular weight compounds that represent models of specific functional groups or moieties within NOM likely to exhibit reactivity toward free chlorine and monochloramine. For example, several different types of aromatic compounds, aliphatic compounds, and amino acids have been studied as examples of popular precursors whose formation potential for C-DBPs and N-DBPs, respectively, has been extensively investigated to provide reaction kinetics and mechanisms of DBP formation. Figure 1.5 shows common model DBP precursors. Details of some noteworthy studies with such precursors for HAA production are briefly discussed below.

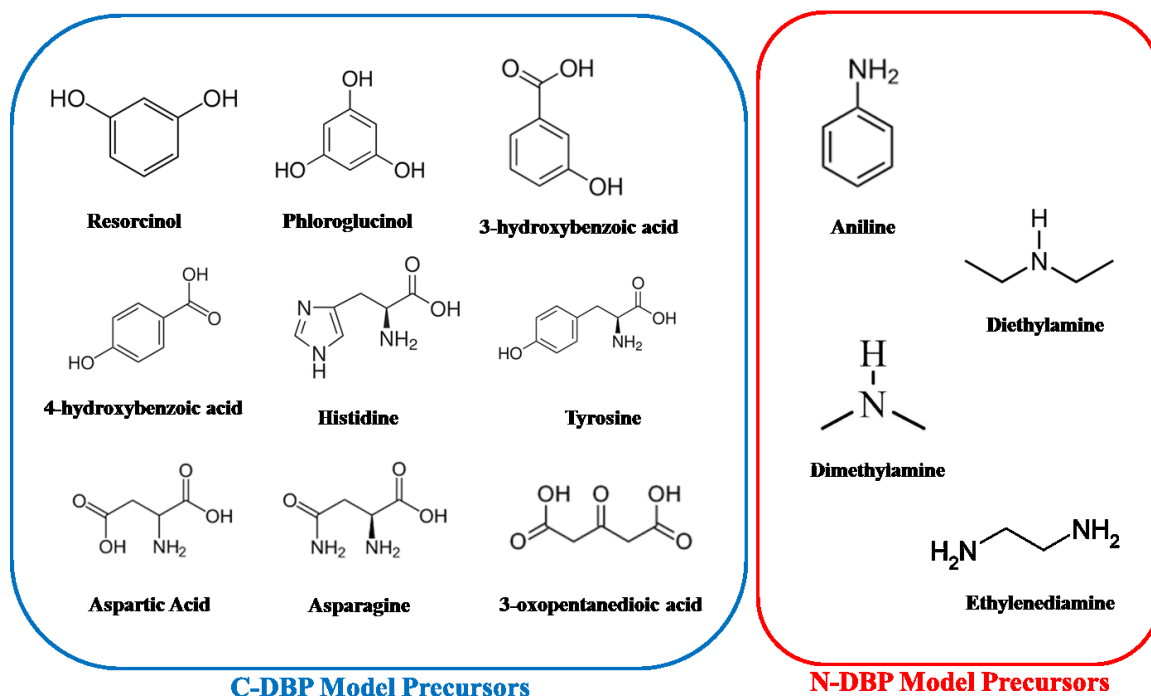


**Figure 1.5.** Compounds commonly used as model precursors for carbonaceous (C-DBP) and nitrogenous (N-DBP) disinfection byproducts.

Chang *et al.* [28] investigated four model compounds for DBP formation: resorcinol, phloroglucinol, 3-hydroxybenzoic acid (3-HBA), and 4-hydroxybenzoic acid (4-HBA), which are shown in Figure 1.4. They found that 3-HBA, 4-HBA, and phloroglucinol produced HAA, with phloroglucinol producing the most. The authors attributed the greater activity of phloroglucinol to its additional -OH group, which lowers its  $pK_a$  and increases SUVA. This work supported results from previous studies that carboxylated substituents tend to generate more HAAs [29-31].

The aliphatic compound  $\beta$ -dicarbonyl acid was studied by Dickenson *et al* [32] as a precursor to THM and HAA formations. As motivation for this work, Reckhow and Singer [25] found that  $\beta$ -dicarbonyl moieties within aromatic and aliphatic compounds represent precursors for DCAA and TCAA. Consistent with these findings, Dickenson *et*

*al.* observed that significant formation of DCAA occurred from the chlorination of  $\beta$ -dicarbonyl acid compounds. Additionally,  $\beta$ -keto-acid type structures exhibited the potential to be slow-reacting DCAA precursors. Thus, for carboxylic acid functional groups, one group must be a carbonyl whilst the other a ketone. If not, DCAA formation will result in smaller yields.

Several studies have also explored amino acids as model precursors to HAA formation. For example, Hong *et al.* examined 20 species of amino acids as precursors for both THM and HAA formation. Ring structured (histidine, phenylalanine, proline, tryptophan, and tyrosine) and chain structured (aspartic acid and asparagine) amino acids exhibited an increase in HAA formation with an increase in chlorine demand. This suggests that the activated ring structure is the primary site for HAA formation [33]. Alternatively, the high HAA production from the two chain linked amino acids was evaluated and modeled in previous studies in which HAAs were produced by a chlorine induced decarboxylation [34, 35]. In another study, Bond *et al* [36] examined 9 NOM surrogates including 5 amino acids, 2 carbohydrates, and 2 phenolic chemical groups. Their work verified an earlier study of Dickenson *et al* [32] that found L-aspartic acid to be a slow-reacting precursor to DCAA. This is likely due to the extra steps required to form  $\beta$ -keto-acid intermediate, which means higher DCAA yields are dependent upon longer chlorination times.

Briefly, several nitrogen containing compounds (see Figure 1.5) have been suggested as precursors to NDMA formation. The most prevalent are amines and amine based polymers. A detailed review of known rate constants of amine compounds for reactions of NDMA with various oxidation species was completed by Sharma [37]. The

review shows several pathways to NDMA formation via the oxidation of amines such as dimethylamine, dimethylethanolamine, and 3-dimethylaminomethyl indole. Additionally, it is evident that the ozonation of polymer based amines (i.e. coagulants and flocculants) produce NDMA via the reaction of the hydroxyl radical on the surface [38].

#### 1.4 Carbon Nanotubes as Next Generation Precursors

Researchers have applied concepts and mechanisms developed by use of specific model precursors to examine the DBP formation potential of emerging pollutants. Studies have shown that DBPs have formed from pharmaceutical drugs, personal care products, pesticides, estrogens, and algal toxins. Many of these contaminants contain activated aromatic rings that are readily oxidizable by disinfectants [39].

Pharmaceutical and personal care products (PPCPs) are endocrine disrupters that constitute a large class of chemical contaminants that originate from human usage and excretion. Several studies on pharmaceuticals such as antibiotics [40], human and veterinary antibacterial agents [41, 42], and antiepileptic drugs [43] have been observed to react with chemical oxidants and ozone to generate DBPs. Additionally, chemicals found in sunscreen [44] and fragrances [45] when chlorinated resulted in DBPs.

Engineered nanomaterials represent another emerging pollutant class, with much work focused on their fate and implications in the environment. With respect to DBP formation, we contend that carbonaceous nanomaterials including carbon nanotubes (CNTs) and related structures like fullerenes and graphene are probable DBP precursors. For example, many of the aforementioned model precursors are evocative of functionalities present on the surface of commercially available CNTs. Due to the

hydrophobic nature of carbon nanotubes, studies have shown they possess the ability to adsorb a wide range of organic contaminants [46, 47].

As CNT production increases, they may become a competitive and supplemental option to activated carbon (AC), which has long been used in water treatment. Previous studies on activated carbon have shown the formation of halogenated by-products [48] and NDMA [49] via the reaction of chlorine on the surface of AC. Since CNTs and AC share several important material properties, similar chlorine reactivities can be expected.

Carbon nanotubes are one-dimensional nanostructures that are formed through the rolling of a graphene sheet into a cylinder of nanoscale diameter [50]. Surface of CNTs can be altered via functionalization to integrate several surface moieties (e.g.  $-\text{OH}$ ,  $-\text{COOH}$ ,  $-\text{C}=\text{O}$ ,  $-\text{NH}_2$ ) that are commonly studied as model DBP precursors [51]. Although CNTs share many of the same properties as AC, the differences in their nanoscale dimensions [52] should enhance their reactivity toward chlorine based disinfectants. Some CNTs are made from a single graphene sheet (SWCNT), which impacts the electronic properties causing them to range from metallic to semi-conducting [50]. This would make SWCNTs to exhibit greater redox activity, likely making them more prone to oxidation via chlorine disinfectants.

Additionally, three other CNT material properties may significantly impact the reactivity towards chlorine disinfectants. First, variations in the purity and elemental composition may provide more reactive sites on which CNTs may contribute to DBP formation [50]. Second, CNTs can be varied by doped materials such as nitrogen (N-CNTs) that make them more efficient at reduction processes [53]. Finally, the surface functionality will certainly influence the reactivity of CNTs. The surface moieties

previously noted have been shown to form DBPs from specific model precursors. For halogenated DBPs, oxide groups such as carboxyl, carbonyl, and hydroxyl [54] will likely play a large part in DBP formation potential.

### 1.5 Overall Objective, Hypothesis, and Specific Aims

The purpose of this study is to determine the extent to which known and regulated disinfection by-products are produced during the chlorination of commercially available carbon nanotubes. Several carbon nanotubes with various surface functional groups were employed to determine how oxidation state affects the formation of DBPs.

We believe that in NOM-free systems, oxidation of CNTs by free chlorine will yield halogenated (THMs, HAAs) and nitrogenous (NDMA) DBPs. The reactivity and yields of these DBPs will be dependent on CNTs properties such as outer-wall structure, presence of dopants, surface chemistry, and purity.

The following specific objectives address whether CNTs are a precursor to disinfection by-products and the goal of minimizing DBP formation in chlorinated waters. These objectives are:

1. Determine if HAAs form via the chlorination of CNTs.
2. Investigate which species of CNTs are more reactive to produce HAAs based on the oxidation state on the surface of the CNTs.
3. Determine the formation of NDMA in the presence of a non N-containing CNT, chlorine, and ethylenediamine.

## CHAPTER 2 MATERIALS AND METHODS

### 2.1 Reagents

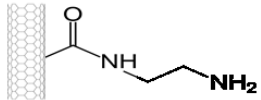
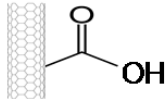
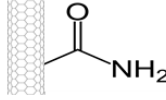
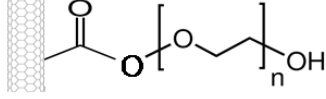
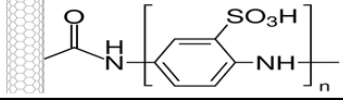
All reagents were used as received. Chlorination experiments used sodium hypochlorite (NaOCl; Fisher; 5.65-6%), anhydrous potassium phosphate monobasic (RPI; ACS grade), sodium hydroxide (Acros Organics; ACS reagent) and sodium sulfite (Sigma Aldrich;  $\geq 98.0\%$ ). Reagents used for chlorine analysis included anhydrous sodium phosphate dibasic (Research Products International Corp.; ACS grade), disodium ethylenediamine tetraacetic acid dehydrate (EDTA; Sigma; ACS grade), ferrous ammonium sulfate hexahydrate (FAS; J.T. Baker®; ACS grade), N,N-diethyl-p-phenylenediamine (DPD; Aldrich; 97% purity) and sulfuric acid (Fisher; ACS Plus). HAA analysis used sulfuric acid, sodium sulfate anhydrous (Fisher; ACS grade), copper II sulfate pentahydrate (Sigma Aldrich,  $\geq 98.0\%$ ), methyl tert-butyl ether (MTBE, Sigma Aldrich, 99.9%), 1,2-dibromopropane in methanol (Crescent Chemicals Co., Inc.), chloroacetic acid (Sigma Aldrich,  $\geq 99.0\%$ ), dichloroacetic acid (Sigma Aldrich, ReagentPlus,  $\geq 99\%$ ), trichloroacetic acid (Sigma Aldrich,  $\geq 99.0\%$ ). NDMA analysis used methylene chloride (DCM; Fisher; stabilized/certified ACS), carbon beads for solid phase extraction (Lewatit AF 5), a 5000  $\mu\text{g/mL}$  NDMA standard in methanol (Sigma-Aldrich; analytical standard), and deuterated NDMA as an internal standard prepared in DCM (NDMA-D6; CIL; 98%). Ethylenediamine analysis used 4-methoxybenzene sulfonyl chloride (Sigma Aldrich,  $\geq 99\%$ ), sodium carbonate (Fisher, HPLC Grade), sodium bicarbonate (Sigma Aldrich,  $\geq 99.5\%$ ), and acetonitrile (Fisher, Optima Grade). All

solutions were prepared in deionized water produced from a Barnstead ROPure Infinity/NANOPure Diamond water system. (Thermo Scientific Barnstead TII).

## 2.2 Carbon Nanotubes

Eight formulations of carbon nanotubes (CNTs) were acquired from NanoLab, Inc. (NL), Carbon Solutions, Inc. (CS), and Cheap Tubes, Inc. (CT). These formulations with surface functionalities (provided by the vendor) are summarized in Table 2.1. These include single-walled (SW) and multi-walled (MW) CNT types with and without (NF) functional groups. Carboxylic acid (COOH), amide (NH<sub>2</sub>), polyethylene glycol (PEG), and m-polyaminobenzene sulfonic acid (PABS) functionalized CNTs were purchased from CS. Amine (NH<sub>2</sub>) functionalized CNTs were purchased from NL. Non-functionalized multi-walled CNTs were purchased from CT (CT MWNF).

**Table 2.1.** List of functionalities of purchased CNTs. Non-functionalized CNTs are not shown.

Vendor	Name	Surface Functionality
Nanolab (NL)	NL SWNH <sub>2</sub>	
Carbon Solution (CS)	CS SWCOOH	
	CS SWNH <sub>2</sub>	
	CS PEG	
	CS PABS	

In addition to as received (or non-functionalized) CNTs, functionalized CNTs were also prepared via oxidation with either concentrated  $\text{HNO}_3$  (N) and a mixture of 70%  $\text{HNO}_3$  and 30% concentrated  $\text{H}_2\text{SO}_4$  (S/N). These functionalization routes are detailed in Oulton et al [55] and were adapted from accepted protocols available in the literature [56]. Briefly, CNTs were suspended in the appropriate concentrated acid solution and were subsequently sonicated for 1 hour to promote CNT dispersion. The mixture was then refluxed for a fixed period of time (1.5 h for  $\text{HNO}_3$  and 8 h for S/N mixtures), after which the acidified suspension was allowed to cool overnight. The CNTs were separated from the cooled suspension by filtration, and the retained CNTs were repeatedly flushed with DI water as a cleaning procedure until the filtrate achieved a pH value above 5. The washed CNTs were dried overnight in an oven at 100 °C, and the resulting powder was pulverized with a mortar and pestle prior to suspensions of the oxidized CNTs in DI water.

The schematic for the synthesis of CS PEG is shown below in Figure 2.1. CS PEG are functionalized via the procedure provided by Zhao et al [57]. Briefly, the CS carboxylated CNTs were sonicated in dimethylformamide (DMF), and then reacted with oxalyl chloride in suspension. PEG was added to the suspension and the mixture was allowed to stir for 5 days at 100 °C. The mixture was allowed to cool and then filtered through vacuum filtration.

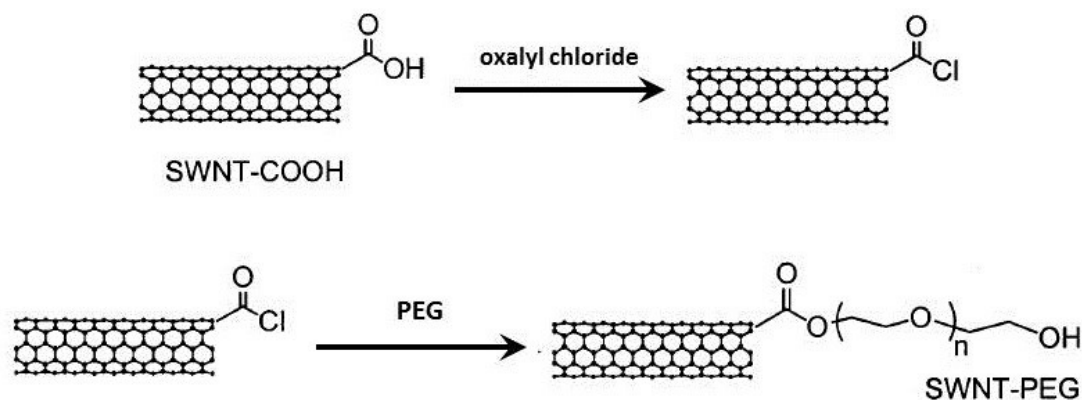


**Figure 2.1.** Schematic of CS PEG functionalization route. Adapted from Zhao *et al* [57].

Finally, additional experiments were conducted with MWCNTs from CheapTubes.com to explore how exposure to common disinfectants influenced DBP formation extended. To simulate processing in engineered treatment systems, non-functionalized CT MWNF was aged via extended and repeated reaction with ozone and germicidal UV light. Briefly, aging with ozone was accomplished by delivering a continuous 0.2 mL/min stream of an  $O_3/O_2$  mixture generated using a Model SS-300 (Pillar Technologies) ozone generator into 50 mL of a 1 g/L suspension for up to 48 h. Prior to reaction with chlorine to measure HAA formation, these ozonated suspensions were left open to air to promote release of any residual ozone. Aging with germicidal UV utilized wavelengths of light from a 200 W Hg(Xe) lamp (Newport Corporation; Model 6290) equipped with a  $>225$  cut-on filter (Newport Corporation; CGA-225).

## 2.3 General Procedures

### *2.3.1 Haloacetic Acid Formation Experiments*

Experiments to measure the rate and yields of HAAs during CNT chlorination were performed in 250 mL glass beakers covered with Parafilm® and aluminum foil to

prevent chlorine decay from light and open air contact. Reactors contained 60 mL of 5 mM phosphate buffer (pH 7 or 8), a CNT loading between 5 – 20 mg/L, and an initial HOCl concentration between 5 – 30 mg/L as Cl<sub>2</sub>. Aqueous stock solutions of free chlorine (HOCl) were prepared by diluting concentrated sodium hypochlorite (Fisher; ~50 g/L as Cl<sub>2</sub>) to ~500 mg/L in amber glass bottles sealed with Teflon-lined screw caps. Stock HOCl solutions were prepared daily, and their concentration was measured via titration prior to use. Prior to use in chlorination experiments, CNTs listed in Table 2.1 were sonicated for at least 10 minutes. The reaction was initiated by spiking in the desired volume of stock CNT suspension into a pH buffered solution of HOCl. Reactors were well-suspended by mixing using a stir bar and stir plate. Samples were taken at various time intervals to measure HAA and HOCl concentrations over time. Aqueous sodium sulfite (Na<sub>2</sub>SO<sub>3</sub>) stock solutions were prepared at a 1 M concentration suspended in DI water, and were made weekly. Samples were quenched with an equivalent sodium sulfite stock solution to residual HOCl concentration, and were stored in the fridge for no more than 5 days before analysis. Control experiments of chlorine only were conducted to normalize chlorine demand, and subtract out peaks that are due to derivatization.

### *2.3.2 N-Nitrosodimethylamine Formation Experiments*

Experiments exploring the mechanism by which NDMA formation is produced during chlorination of N-CNT suspensions were performed using the protocols described for HAAs except ethylenediamine was also introduced into the reactors. Reactors contained 60 mL of 5 mM phosphate buffer (pH 7 or 8), a N-CNT loading between 5 – 20 mg/L, an initial HOCl concentration between 5 – 30 mg/L as Cl<sub>2</sub>, and EDA concentrations ranged between 200 – 5000 µg/L. The reaction was initiated by spiking in

the desired volume of stock N-CNT suspension into a pH buffered solution of HOCl. During reaction, reactor contents were well-suspended by mixing using a stir bar and a stir plate, while samples were periodically withdrawn to monitor NDMA and HOCl concentrations over time. Samples were quenched with an equivalent sodium sulfite to residual HOCl concentration, and were stored at 4 °C for no more than 5 days before analysis. HOCl and monochloramine concentrations were measured via titration prior to analysis. Control experiments were conducted using CNT suspension and HOCl, CNT and EDA, and EDA and HOCl. These were performed to measure and normalize chlorine demand, and to determine the source of NDMA production.

### *2.3.3 Ethylenediamine Sorption Experiments*

Experiments were performed using the protocols described for HAAs and NDMA except no chlorine was introduced into the reaction. CNTs were reacted with EDA in 10 mL batch systems using 20 mL headspace vials, grey butyl stoppers, and Al crimp top seals (all from Wheaton Industries Inc.). Mixing was done by inverting vials at 60 rpm using a Model RT50 rotator (Cole-Parmer Instrument Company; Roto-Torque). Reactors contained 10 mL of 5 mM phosphate buffer (pH 7 or 8), PEGylated CNT loaded at 10 mg/L, and EDA concentrations between 200 – 5000 µg/L, and allowed to mix for 24 h. After mixing, CNTs were filtered using 1 mL syringe filters.

## 2.4 Analytical Methods

### *2.4.1 HOCl Titrations*

Chlorine and monochloramine concentrations were determined using the Standard Method 4500-C1 F DPD-FAS titrimetric method [58] Titrations were prepared by adding

5 mL of phosphate buffer reagent and N,N-Diethyl-p-phenylenediamine (DPD) indicator solution to 100 mL of diluted sample, with the solution turning pink to red in hue in the presence of free chlorine. The free chlorine concentration was then quantified by titration with ferrous ammonium sulfate (FAS) until the red color disappeared. Monochloramine was quantified by adding potassium iodide crystals to the titration flask after titrating for free chlorine to produce the same color hue which was again titrated to clear with FAS.

#### *2.4.2 Haloacetic Acid Analysis*

The concentration of HAAs in samples was analyzed using the method developed by Xie *et al.* [59]. Briefly, A 35 mL sample from the experimental reactor was transferred into a 50 mL amber bottle sealed with PTFE-lined screw caps. Concentrated sulfuric acid (1.75 mL) was then added to drop the pH of the solution below 0.5. Next, 14 grams of sodium sulfate anhydrous ( $\text{Na}_2\text{SO}_4$ ) was immediately added and the mixture was vigorously shaken by hand until the salt was completely dissolved. This was followed by the addition of 1.75 grams of copper sulfate pentahydrate ( $\text{CuSO}_4 \cdot 5\text{H}_2\text{O}$ ), and the mixture was once again shaken until the salt entirely dissolved. Finally, 4 mL of methyl tert-butyl ether (MTBE) was added to the solution, along with 20  $\mu\text{L}$  of 1,2-dibromopropane at 5  $\mu\text{g}/\text{L}$  in MTBE, which was used as an internal standard.

Samples were placed on a mechanical shaker (Lab Line; Orbital Shaker) at 150 rpm for 30 minutes. Next, the samples were methylated by transferring 3 mL of the upper MTBE layer into a 15 mL amber vial with PTFE-lined screw caps. Subsequently, 2 mL of 10% sulfuric acid in methanol was added to each vial. The vials were capped and placed into a water bath (50°C) for 2 hours, after which they were removed and allowed to cool to room temperature. Then, 5 mL of 10% sodium sulfate solution was added to

each vial and shaken by hand for 2 minutes. The emulsion was allowed to settle and 1 mL of the upper MTBE layer was extracted and was transferred to a 2 mL GC autosampler vial for immediate analysis.

HAAAs were measured by an HP 6890N gas chromatograph (GC; Agilent Technologies, Inc.) coupled with a G2397A electron capture detector (ECD; Agilent Technologies, Inc.). A 3  $\mu$ L sample was injected into the GC in splitless mode and separated on a 30 m length, 0.25 mm i.d., and 0.25  $\mu$ m film thickness DB-5 column. Temperature ramps were as follows: 35  $^{\circ}$ C for 10 minutes, 35 – 75  $^{\circ}$ C at 5  $^{\circ}$ C/minute, 75  $^{\circ}$ C for 15 minutes, 75 - 100  $^{\circ}$ C at 5  $^{\circ}$ C/minute, 100  $^{\circ}$ C for 5 minutes, 100 - 135  $^{\circ}$ C at 5 $^{\circ}$ C/minute, and 135  $^{\circ}$ C for 5 minutes. The injector temperature was 200 $^{\circ}$ C. Nitrogen was used as the carrier gas at 1 mL/minute (constant flow). The ECD was set at 250  $^{\circ}$ C.

#### *2.4.3 N-Nitrosodimethylamine Analysis*

NDMA was analyzed according to standard methods [58]. A 50 mL sample was transferred to a 200 mL amber bottle with a screw cap. A 100  $\mu$ L aliquot of internal standard (NDMA-d6) solution was added to all samples to achieve a concentration of 800 ng/L. Approximately 200 mg of carbon beads was then added to the solution and allowed to mix on a mechanical shaker for 1 hour. The carbon beads were removed subsequently using vacuum filtration using circle, 0.11  $\mu$ m, filters (Whatman; Grade 1 filter paper). Filters containing the carbon beads were placed in aluminum weigh boats and allowed to dry for 30 minutes. The beads were transferred into 2 mL GC autosampler vials and 600  $\mu$ L of dichloromethane was added to each vial for NDMA extraction.

NDMA was measured by an HP 6890 gas chromatograph coupled with an HP5973 mass selective detector. A 2  $\mu$ L sample was introduced into the GC by a split

injection. The front inlet are as follows: initial temperature set at 50 °C, pressure 3.8 psi, split ratio 50:1 with helium as the gas carrier. The oven was set at an initial temperature of 40 °C for 2 minutes, then the temperature was ramped up to 60 °C at 10 °C. The capillary column's dimensions were 30 m length, 250 µm diameter, and 0.25 µm film thickness, and was an Agilent 19091J-433 HP-5 5% phenyl methyl siloxane column. Selective ion monitoring was used to quantify characteristic peaks of NDMA at m/z 75 and NDMA-d6 at m/z 81. A method detection limit of 3 ng/L was determined.

#### *2.4.4 Ethylenediamine Analysis*

Ethylenediamine (EDA) was measured via UV absorbance after chemical derivatization with 4-methoxybenzene sulfonyl chloride. This method was adapted from Mitch et al [60]. Samples from EDA sorption experiments (3 mL) were first buffered by adding 0.5 mL of a 20 mM Na<sub>2</sub>CO<sub>3</sub> solution and 0.5 mL of a 20 mM NaHCO<sub>3</sub> solution prepared in DI water, and then mixed with 1.5 mL of acetonitrile to enhance the solubility of the derivatizing agent. The mixture was then spiked with 9 µL of a 500 mg/L 4-methoxybenzene sulfonyl chloride stock solution prepared in acetone, and the mixture was then placed on a shaker overnight. Analytes were detected by UV absorbance at 287 nm in a quartz cuvette.

Calibration samples of the EDA range (200 – 5000 µg/L) were derivatized prior to CNT samples. Absorbance levels were measured and the molar absorptivity for each known concentration was calculated using Beer's Law equation. A calibration curve was developed and used for comparison in CNT samples. Control samples of EDA only were performed to determine if filtering removed any EDA from the resulting solution.

## CHAPTER 3 HALOACETIC ACID FORMATION DURING CHLORINATION OF CARBON NANOTUBES

### 3.1 Introduction

Previous work conducted by Verdugo et al [61] demonstrated that nitrogen containing carbon nanotubes (N-CNTs) can serve as a precursor to nitrogenous disinfection byproducts (DBPs), specifically N-nitrosodimethylamine (NDMA). The formation of NDMA is directly tied to the nature of the surface groups added to the CNT surface, which serve as a reservoir of nitrogen for formation of nitrogenous disinfection byproducts. However, the environmental implications for the work of Verdugo et al. are somewhat limited because N-functionalized CNT have yet to be extensively used in commercial products or industrial processes.

In a more recent study by Verdugo [62], the potential for other classes of CNTs to generate disinfection byproducts (DBP) during chlorination was explored, particularly other types of CNTs with surface groups analogous to suspected model precursors for DBPs (as discussed in Chapter 1). These included both non-functionalized (i.e., as-received) CNT powders, oxidized CNT powders, primarily with surface carboxylic acid groups, and polymer functionalized CNTs (CNTs coated with a PEG or PABS layer) from various commercial vendors. These CNTs are more representative of those used currently in commercial and industrial application including their use in sensors, electronics, composites, and energy storage. Therefore, they represent the CNTs most likely to be discharged into the environment, make their way into source and wastewaters, or be integrated into next generation water treatment technologies (e.g., CNT enforced membranes).

For these CNTs, Verdugo explored their reactivity toward chlorine, and their role as a precursor to the formation of chloroform, a trihalomethane (THM) commonly generated as a byproduct of chemical disinfection of water containing organic matter. Generally, Verdugo found that chloroform was produced to the greatest extent on polymer functionalized CNTs, as was also observed for NDMA formation with N-containing surface polymers (e.g., PABS). Chloroform was only produced to a very modest extent on PEGylated CNTs,  $0.75 \mu\text{g-CHCl}_3/\text{mg-CNT}$ , but he did observe that the manner in which the CNTs were oxidized influenced their propensity to generate chloroform. Most notably, surface oxidation via extended ozonation increased the ability of CNTs to produce chloroform more so than CNTs oxidized by other methods (e.g., refluxing with strong acid).

This work extends the prior work of Verdugo by considering the potential of these same types of CNTs to generate another common class of DBP, haloacetic acids (HAAs). We quantified the production of mono-, di-, and trichloroacetic acid (MCAA, DCAA, and TCAA, respectively) generated via the chlorination of CNTs. We explored the influence of the bulk CNT properties (e.g., comparing formation on single-walled versus multi-walled CNTs), surface chemistry (e.g., non-functionalized versus carboxylated CNTs) and extent of environmental processing (e.g., extended ozonation, UV exposure) on HAA formation. We also considered the production of HAAs from polymer functionalized CNTs such as PABS and PEG, which previously have been implicated as the largest producer of DBPs during chlorination of functionalized CNTs. Results are presented in the context of comparing HAA formation to chloroform formation from

earlier results from Verdugo, while also considering the net amount of combined DBPs (i.e., the cumulative total of NDMA, chloroform and HAAs) during chlorination.

### 3.2 HAA Production during Chlorination of Various Carbon Nanotube Formulations

Figure 3.1 reveals the fraction of initial chlorine remaining after 4 h of reaction for the types of CNTs considered herein. CNTs were chlorinated in batch reactors at pH 8 in 5 mM phosphate buffer for 4 h. We note that chlorine decay data presented in the figure were corrected by subtracting the chlorine demand measured in a control system that had no CNTs present in solution. Figure 3.1 is organized to compare similar CNT functionalities among the vendors. Purple are non-functionalized, green are nitrogenated, blue are acid-oxidized, and red are polymer coated CNTs. Multi-walled (MW) CNTs contain a diagonal pattern bar while single-walled (SW) CNTs are a solid color bar. CNTs utilized include single-walled (SW) and multi-walled (MW) CNT types with and without (NF) functional groups. Carboxylic acid (COOH), amide (NH<sub>2</sub>), polyethylene glycol (PEG), and m-polyaminobenzene sulfonic acid (PABS) functionalized CNTs were purchased from CS. Amine (NH<sub>2</sub>) functionalized CNTs were purchased from NL. Non-functionalized multi-walled CNTs were purchased from CT (CT MWNF). CNTs purchased from all three vendors were oxidized with nitric acid (N) or a sulfuric acid and nitric acid mixture (SN).

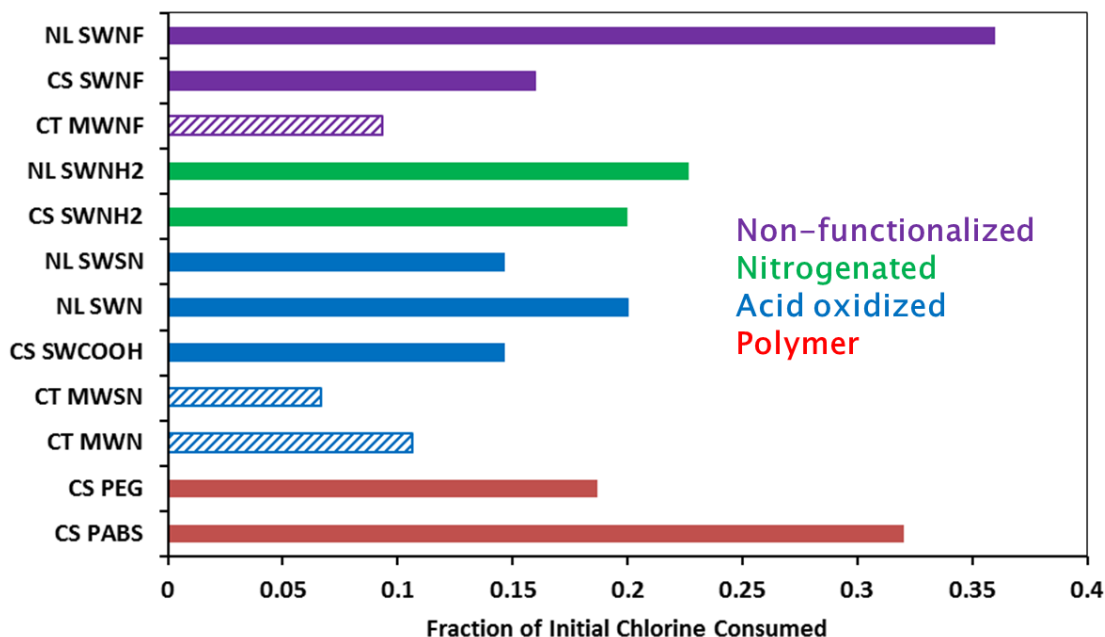


**Figure 3.1.** Fraction of initial chlorine consumed after 4 h of reaction for all CNTs considered herein. Experiments were conducted in 5 mM phosphate buffer of 10 mg/L CNT loading and 15 mg/L HOCl dose.

For non-functionalized CNTs, NL SWNF exhibited the highest chlorine reactivity. This is likely due to the  $sp^2$  hybridized carbon centers on the CNT surface being more reactive towards chlorine than some other, which are more oxidized sites. The N-CNTs purchased from NL and CS exhibited about the same chlorine consumption. Oxidized CNTs that were functionalized with nitric acid displayed the greatest chlorine reactivity for SW and MW CNTs. NL CNTs oxidized with a sulfuric acid and nitric acid mixture consumed the same amount of chlorine as CS SWCOOH. In the polymer coated CNTs, CS PABS consumed nearly twice as much chlorine as CS PEG. The high reactivity for CS PABS is likely due to the secondary amines and aromatic moieties in the polymer, which has been shown to be active towards chlorination [1]. For all of the

CNTs, MW CNTs consumed the lowest amount of chlorine compared to their SW counterparts.

Table 3.1 shows HAA formation via the chlorination of CNTs and the chlorine demand associated with each CNT. When the signal in the control was greater than the CNT samples, it was presumed there was no HAA generation.

**Table 3.1.** MCAA, DCAA, TCAA, and total HAA formation in  $\mu\text{g-HAA/mg-CNT}$  and the corresponding chlorine consumption. CNTs that did not produce detectable limits of HAAs are listed as ND. CNTs that did produce HAAs, but were not quantifiable are listed as NQ. Chloroform (CF) data were provided by Verdugo [62]. Experiments were conducted in the same conditions as Figure 3.1.

Sample	MCAA	DCAA	TCAA	THAA	CF	Fraction of Initial Chlorine Consumed
CS PABS	110.5 $\pm$ 47.4	3.9 $\pm$ 1.3	6.3 $\pm$ 2.1	169.4 $\pm$ 47.5	3.46 $\pm$ 0.81	0.32
CS PEG	15.5 $\pm$ 2.6	0.8 $\pm$ 0.3	0.8 $\pm$ 0.2	20.1 $\pm$ 2.6	0.75 $\pm$ 0.09	0.19
CS SWCOOH	3.7 $\pm$ 2.1	0.4 $\pm$ 0.3	0.3 $\pm$ 0.2	6.9 $\pm$ 2.2	ND	0.15
CT MWN	2.1 $\pm$ 1.4	NQ	NQ	4.3 $\pm$ 1.4	ND	0.11
NL SWN	6.2 $\pm$ 1.9	NQ	0.25 $\pm$ 0.06	8.6 $\pm$ 1.9	ND	0.20
CT MWSN	3.2 $\pm$ 2.1	0.5 $\pm$ 0.3	0.6 $\pm$ 0.1	6.6 $\pm$ 2.1	ND	0.07
NL SWSN	6.7 $\pm$ 0.9	0.4 $\pm$ 0.1	0.7 $\pm$ 0.09	8.8 $\pm$ 0.9	ND	0.15
CS SWNH2	6.1 $\pm$ 0.2	0.3 $\pm$ 0.2	0.2 $\pm$ 0.05	7.1 $\pm$ 0.3	0.1 $\pm$ 0.03	0.20
NL SWNH2	NQ	0.2 $\pm$ 0.1	ND	0.6 $\pm$ 0.3	ND	0.23
CS SWNF	ND	NQ	NQ	NQ	ND	0.16
CT MWNF	NQ	NQ	NQ	NQ	ND	0.09
NL SWNF	ND	NQ	NQ	NQ	ND	0.36

The greatest degree of HAA formation was observed during the chlorination of polymer functionalized-CNTs, with CS PABS and CS PEG producing 170 and 20  $\mu\text{g}$  total HAAs per mg CNT, respectively. Another notable observation was that oxidation of CNTs, which introduces primarily surface carboxylic acid groups in addition to carbonyl (-C=O) and hydroxyl (-C-OH) moieties, increased their propensity to generate HAAs. Superficially, all oxidized CNTs produced measurable quantities of HAAs, while their non-functionalized analogs (i.e. CS SWNF, CT MWNF, NL SWNF) did not produce any

significant levels of HAAs. For N-containing functionalities, results were varied; while amide functionalized CNT (CS SWNH<sub>2</sub>) formed HAAs, amine-functionalized CNT (NL SWNH<sub>2</sub>) did not. This implies, as was the case with NMDA formation, that the nature of the surface site will strongly influence DBP formation.

In all of the functionalized CNTs, MCAA dominates HAA generation except for NL SWNH<sub>2</sub>. For the polymer coated CNTs, more TCAA is generated than DCAA for CS PABS, while more DCAA is generated than TCAA for CS PEG. In the oxidized CNTs, more TCAA is formed than DCAA. This matches up with what was found in similar model precursors, which is discussed below. The amide CNT (CS SWNH<sub>2</sub>) produces HAA levels and trends similar to those of oxidized CNTs, but the amine CNT (NL SWNH<sub>2</sub>) does not produce any significant levels of HAAs.

Knowing CNT surface moieties, we can predict how CNTs compare to specific model precursors for HAA generation. Literature has shown that compounds with high content of aromatic rings, phenolic hydroxyl groups, and conjugated double bonds are generally the largest source of HAA formation [24]. CNT surfaces can be viewed as containing aromatic rings throughout the entire structure. However, their rigid physical structure makes them impervious to DBP formation during chlorination, rather requiring surface functional groups and defects for points of attack. This explains why we see no HAA formation from non-functionalized CNTs.

CS PABS was the only CNT analyzed that contained an additional aromatic ring attached with the functional group. The high reactivity of CS PABS likely originates from the secondary amine and aromatic moieties in the polymer. Formation of HAAs from CS PEG is perhaps due to either the functionalization procedure during which a

variety of precursors could be generating as a result of wall etching due to acid refluxing and/or nucleophilic acyl substitution during halogenation of CNT carboxyl groups, or the PEG moiety may produce HAAs when chlorinated without CNTs present.

Several model precursors similar to those found on oxidized CNTs have been studied for HAA formation. Model precursors such as 3-hydroxybenzoic acid and phloroglucinol [28], and 4-hydroxybenzoic acid [63], 3-oxopentanedioic acid, ferulic acid, and sinapic acid [64] all have carboxyl groups attached and have shown to generate significant amounts of HAAs. Carboxylic acids of five to nine carbons are hydrophobic fractions which lead to HAA formation [26].

Ring structured amino acids such as tyrosine [33] have been shown to generate more HAAs than most non-aromatic amino acids. The amino acid model precursor asparagine [33] is one precursor similar in structure to surface groups on CS SWNH<sub>2</sub>. One possible difference between the two N-CNTs relates to the amount of surface oxygen on the surface. Another factor affecting HAA formation might stem from the differences in amine versus amide. Amides (which have N-C=O) may be more prone as Cl attacks at the N, which could liberate C=O groups for subsequent reaction and conversion to HAAs. Also, aliphatic amines are typically more hydrophilic, which do not generally produce HAAs [26].

### 3.3 Influence of Experimental Parameters on HAA Formation

To explore whether HAA formation was limited by availability of carbon or the amount of free chlorine in our systems, experiments were conducted that varied CNT loading and measured corresponding HAA formation over time. Figures 3.2, 3.3, and 3.4 show MCAA, DCAA, and TCAA formation, respectively, for all CNTs at 5, 10, and 20

mg/L CNT loading. Polymer CNTs (CS PEG and CS PABS) were plotted on a different figure due to HAA yields being several magnitudes higher than as-received, acid oxidized, and N-CNTs.

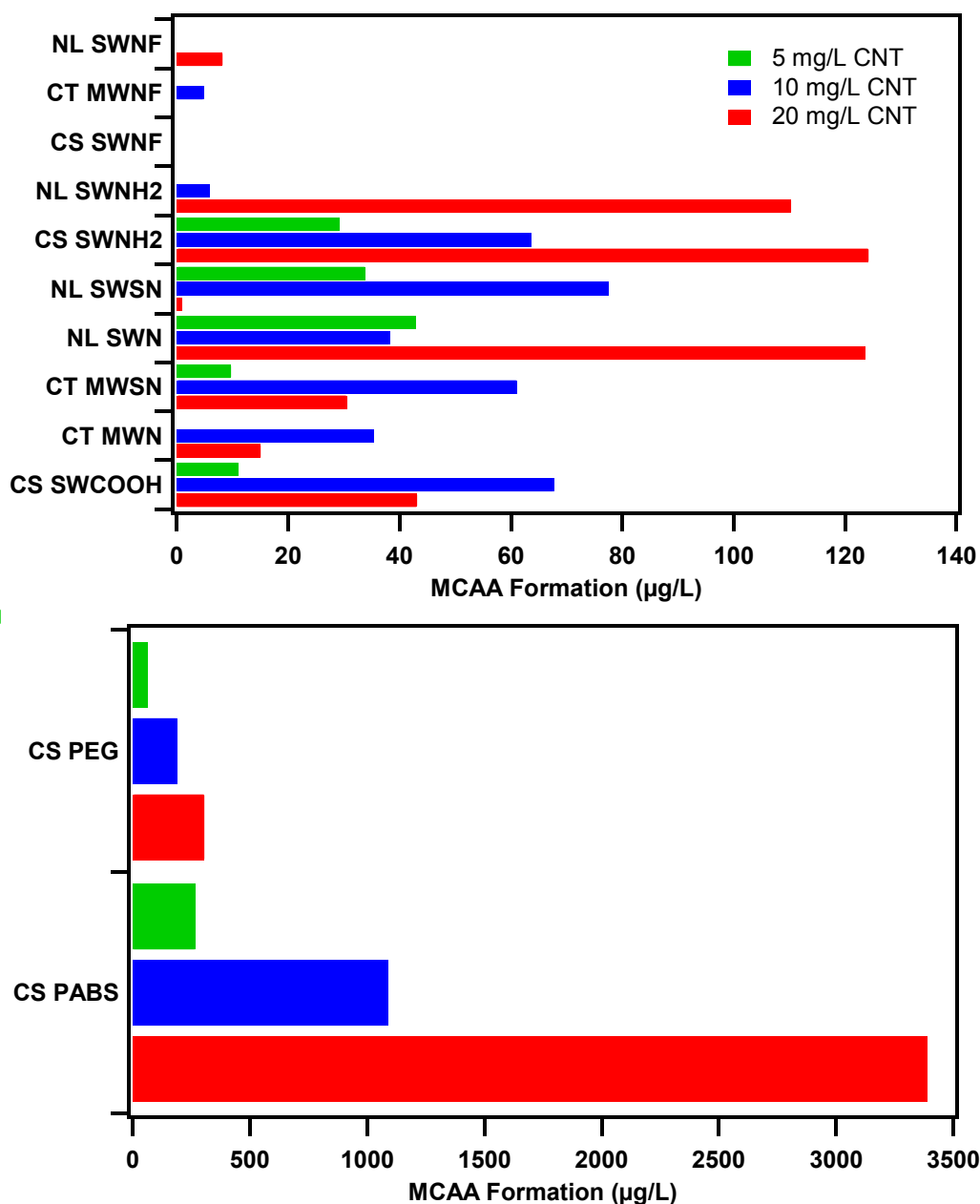


**Figure 3.2.** MCAA formation for varied CNT loadings of 5, 10, and 20 mg/L. Experiments were conducted in 5 mM phosphate buffer with 15 mg/L HOCl, and reacted for 4 hours. The upper figure shows non-functionalized, nitrogenated, and carboxylated CNTs, while the lower figure shows the polymer functionalized CNTs.

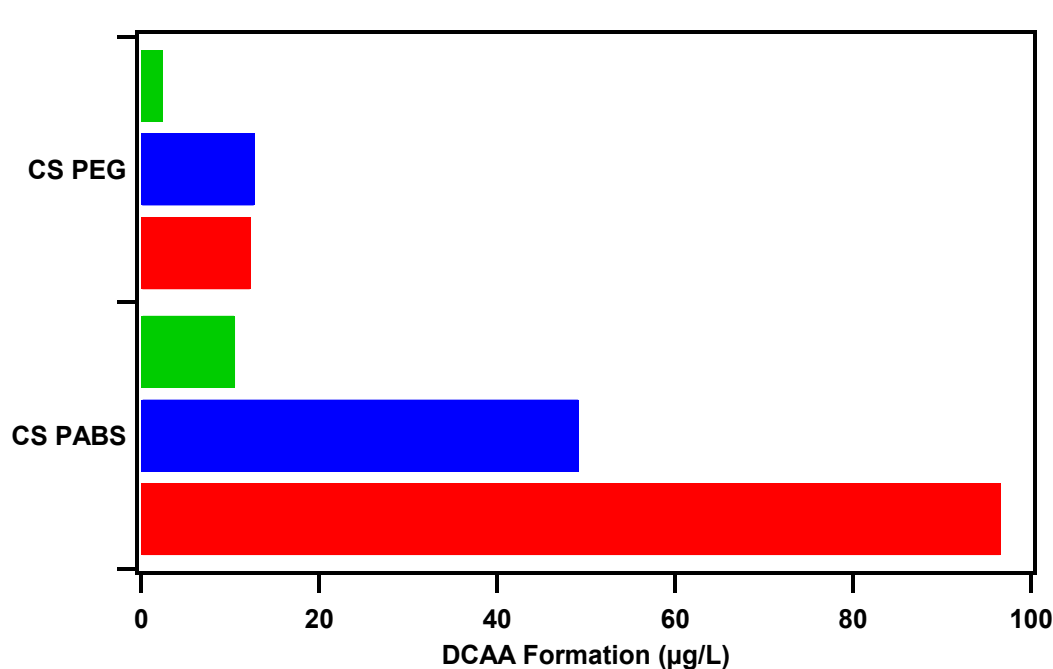
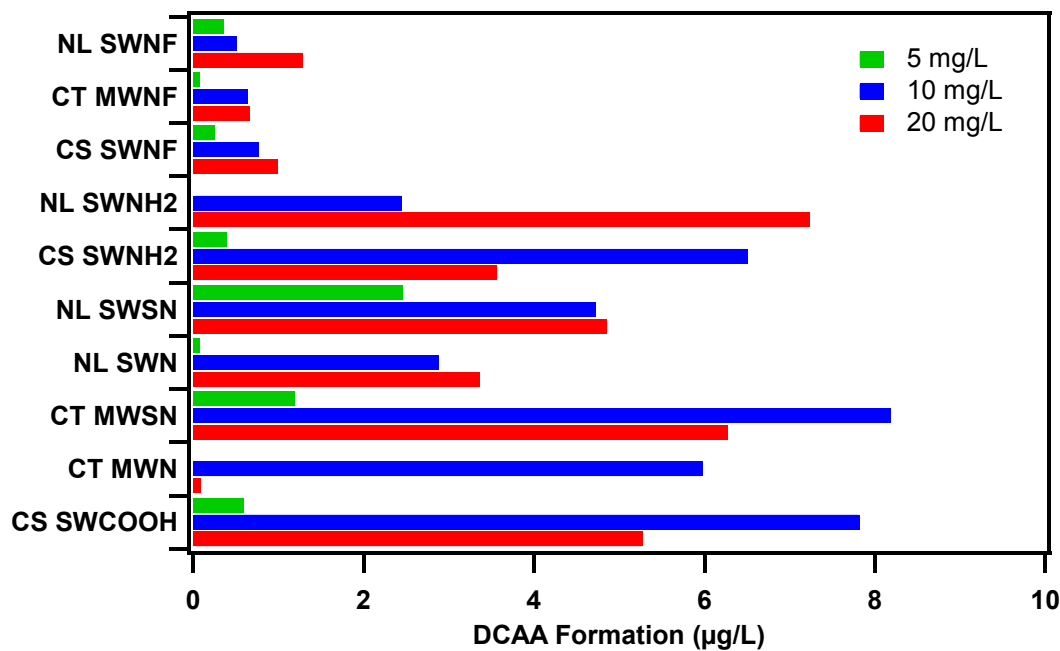


**Figure 3.3.** DCAA formation for varied CNT loadings of 5, 10, and 20 mg/L. Experiments were conducted in 5 mM phosphate buffer with 15 mg/L HOCl, and reacted for 4 hours. The upper figure shows non-functionalized, nitrogenated, and carboxylated CNTs, while the lower figure shows the polymer functionalized CNTs.

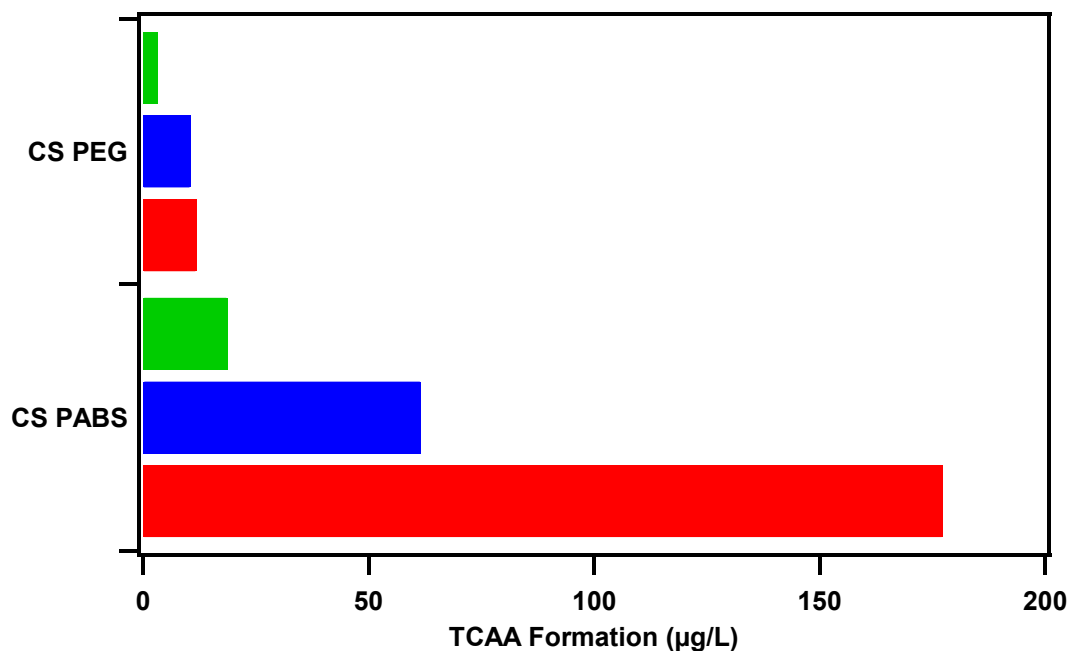
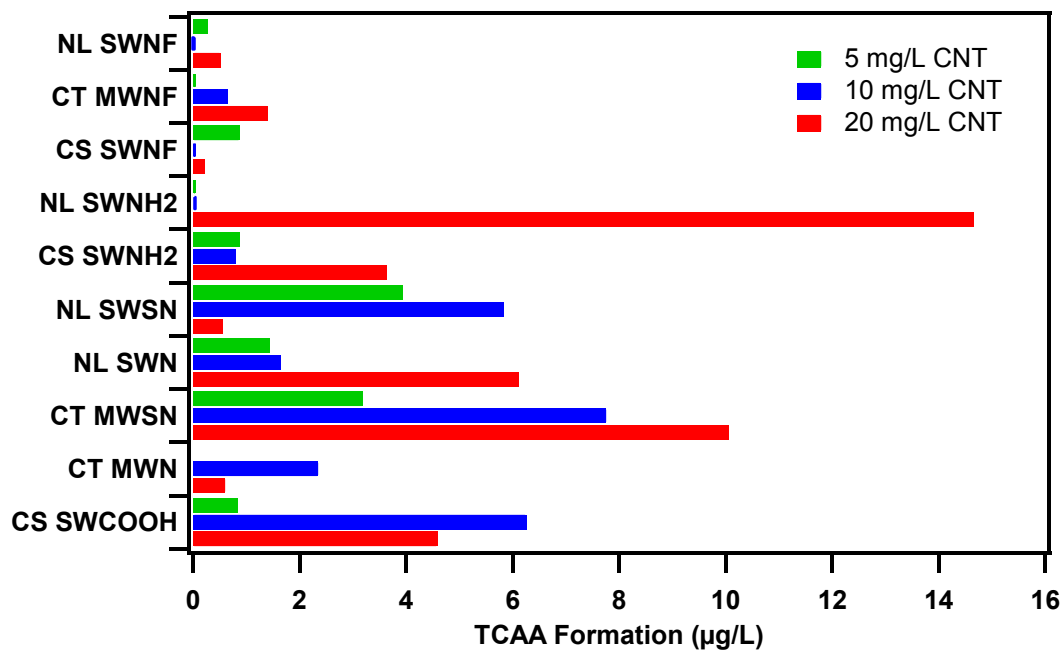


**Figure 3.4.** TCAA formation for varied CNT loadings of 5, 10, and 20 mg/L. Experiments were conducted in 5 mM phosphate buffer with 15 mg/L HOCl, and reacted for 4 hours. The upper figure shows non-functionalized, nitrogenated, and carboxylated CNTs, while the lower figure shows the polymer functionalized CNTs.

There are two trends evident from these figures based on different families of CNTs. In the polymer functionalized, as-received, and N-CNTs, all three HAAs increased with an increase in CNT loading. However, in the acid oxidized CNTs, HAA generation increased when solid loading was increased from 5 to 10 mg/L, but then decreased when solid loading was increased from 10 to 20 mg/L.

As-received CNTs only consistently yielded DCAA and TCAA as solid loading was increased. However, compared to other CNTs at the same loading, HAAs were produced at significantly lower levels. Although there are not any functional groups attached to the surface, these CNTs exhibit chlorine consumption, presumably resulting in surface oxides rather than HAAs, which may help us understand why there are small amounts of DCAA and TCAA production.

As N-CNTs solid loading was increased, formation of HAAs also increased. Interestingly, NL SWNH2 did not produce measurable HAAs until the solid loading was increased to 20 mg/L. This may be due to limited formation that is below our analytical detection limit at lower solid loadings. Chlorination of amino acids typically generate more DCAA than TCAA [33], although tyrosine produces more TCAA which is similar to results we found in CS SWNH2.

Polymer coated CNTs significantly produced more MCAA than DCAA or TCAA. HAA production trends are similar to those found in the previous two families of CNTs, in which all three HAAs increase with surface loading, as expected. For CS PEG, HAA yields for DCAA and TCAA are similar at 10 and 20 mg/L solid loading.

Trends in the acid oxidized CNTs were completely different than those identified in other CNT families. In the CT and CS CNTs, DCAA and TCAA concentrations increase from 5 to 10 mg/L solid loading, but then decrease from 10 to 20 mg/L solid loading. This is a result that is reproducible, and likely speaks to a more complicated HAA formation mechanism on these oxidized surfaces. It could be that the greater demand of chlorine at higher CNT loading limits the amount available in solution to reactive with necessary intermediates in HAA formation.

### 3.4 HAA Formation Kinetics

The rate of chlorine consumption and HAA formation was investigated more closely for CS SWNF, CS SWCOOH, and CS PABS, chosen as representative non-functionalized, oxidized and polymer coated CNT samples, respectively. CS PABS and CS SWCOOH were chosen because they were the most reactive CNTs with respect to HAA formation among the different variations of polymer-coated and surface oxidized (i.e., carboxylated) CNTs, respectively. CS SWNF was reacted to examine whether HAAs were produced over long timescales than utilized in reporting the data in Table 1 (which was collected after 4 h of reaction). However, we did not see any HAA generation over the longer (48 h) timescale.

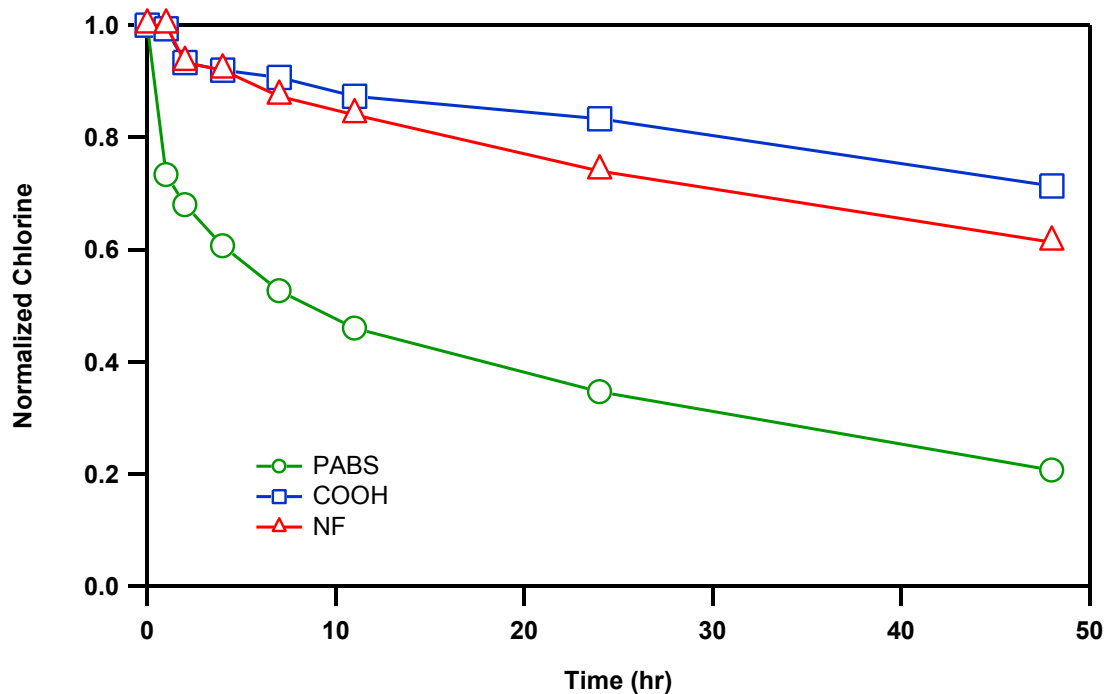


**Figure 3.5.** Chlorine decay kinetics for CS PABS, CS SWCOOH, and CS SWNF. Experiments conducted at pH 8 5 mM phosphate buffer with 10 mg/L CNT loading and 15 mg/L HOCl. Samples were taken at 1, 2, 4, 7, 11, 24, and 48 h.

Figure 3.5 shows the relative rate of HOCl decay in these three CNT systems over 48 h. Consistent with results in Figure 1 and Table 1, CS SWNF exerted a slight chlorine demand (40% removal after 48 h), but resulted in no detectable HAA formation. In contrast, despite showing less chlorine demand (30% removal after 48 h), CS SWCOOH produced measurable HAAs, and the concentration of MCAA, DCAA, and TCAA in these systems continued to increase over the entire 48 h reaction period. Collectively, this implies that the CS SWCOOH surface has an excess of sites reactive toward chlorine, but that the relatively modest reactivity of these sites (as evidenced by the slow rate of chlorine decay in these systems) enables CS SWCOOH to potentially function as a long-term, persistent source of HAAs over time. Figure 3.6 shows the formation of specific HAAs for CS SWCOOH, while Figure 3.7 shows the same results for CS PABS.

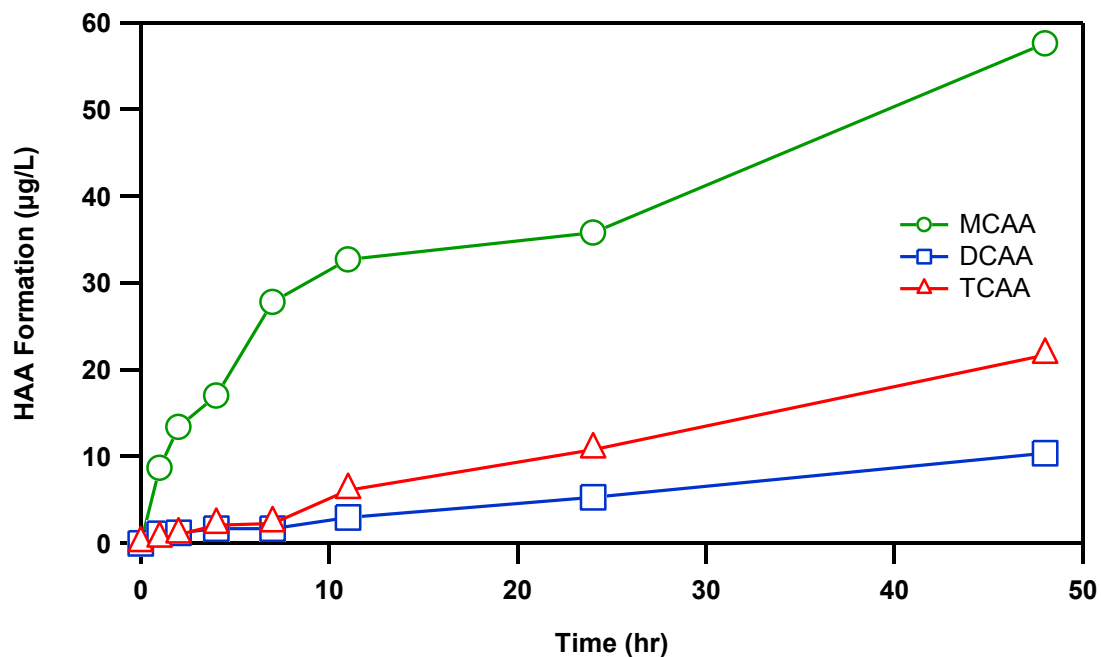


**Figure 3.6.** HAA formation kinetics for CS SWCOOH. Experiments conducted at pH 8.5 mM phosphate buffer with 10 mg/L CNT loading and 15 mg/L HOCl. Samples were taken at 1, 2, 4, 7, 11, 24, and 48 h.

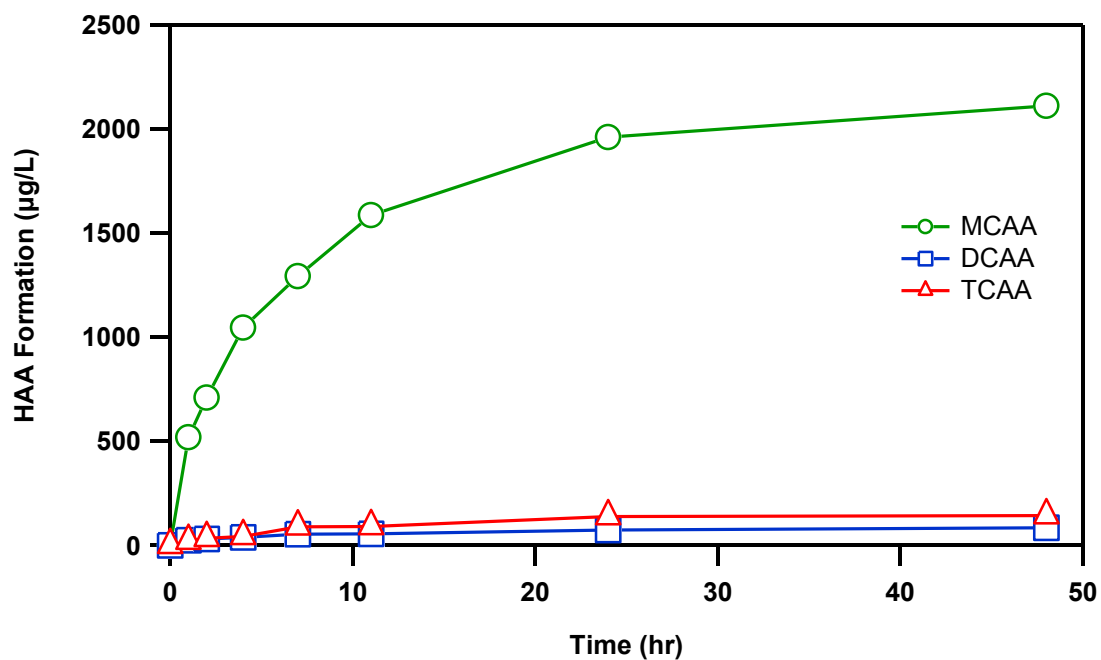


**Figure 3.7.** HAA formation kinetics for CS PABS. Experiments conducted at pH 8.5 mM phosphate buffer with 10 mg/L CNT loading and 15 mg/L HOCl. Samples were taken at 1, 2, 4, 7, 11, 24, and 48 h.

For CS SWCOOH, MCAA is the most abundant HAA species, but is not as dominant as in CS PABS. After 48 hours of reaction time, about 90  $\mu\text{g/L}$  of total HAAs were generated. Over time, the percentage of total HAA present as MCAA decreases. After the first hour, nearly 85% of the total HAAs consists of MCAA, but after 48 hours that percentage decreases to 65%. MCAA is the most prevalent species followed by TCAA, while DCAA is least abundant. CS SWCOOH produced MCAA five times and TCAA twice as much as DCAA, respectively. The chlorine demand and HAA production trends for these CNTs are similar to those reported in a study with 3-hydroxybenzoic acid and 4-hydroxybenzoic acid [28], suggesting that similar reactions may be resulting on CNT surfaces as those proposed for dissolved model organic precursors of HAAs.

In contrast to the sustained production of HAAs in CS SWCOOH suspensions, results from CS PABSs are most consistent with a more limited number of highly reactive sites that yield HAA during chlorination but become exhausted over time. Consistent with earlier reported results, CS PABS exerts the largest chlorine demand, with the chlorine concentration in these suspensions steadily decreasing over the entire 48 h period (80% chlorine consumption). Notably, the rate of chlorine consumption is greatest early on (within the first 10 h) and slows thereafter. The time-dependent trend in HAA formation is different, however, with an initially rapid rate of HAA production eventually slowing to a near halt by 24 h. Indeed, while total HAA concentration is essentially constant from 24 to 48 h, available chlorine drops by  $\sim 10\%$ . Unlike CS SWCOOH, which shows relatively consistent HAA production with chlorine consumption, the ability of CS PABS to yield HAAs becomes exhausted over time, consistent with consumption of specific reactive surface sites functioning as HAA

precursors. Alternatively, a subset of sites CS PABS surface that react with chlorine, albeit more slowly, do not result in HAA formation.

MCAA dominated HAA formation for CS PABS when chlorinated. Over 90% of the total HAAs were MCAA during all time intervals. In the first four hours, CS PABS generates equivalent DCAA and TCAA concentrations, after which TCAA production increases. The ratio of TCAA to DCAA after 48 hours is about 1.7, while MCAA production is twenty five times the amount of DCAA.

Figure 3.8 shows that despite the eventual exhaustion of HAA formation in CS PABS systems, the polymer-coated CNTs produce HAAs far more readily (per unit of chlorine consumed) than oxidized CNTs. Data in Figure 3.8 show total HAA formation (in  $\mu\text{g}$ ) normalized to the amount of chlorine consumed at that same point along the reaction progress (with normalized HAA formation data shown as a function of time across 48 h). This value essentially represents an effective yield of HAA per unit of chlorine demand for each type of CNT. Consistent with the constant HAA production over time in CS PABS suspensions, we see that HAA yields in CS SWCOOH remain constant while chlorine continues to be consumed. Averaging out both graphs, we observed that CS PABS produces  $67.9 \mu\text{g-HAA/mg-Cl}$  consumed, while CS SWCOOH produces  $6.3 \mu\text{g-HAA/mg Cl}$  consumed.

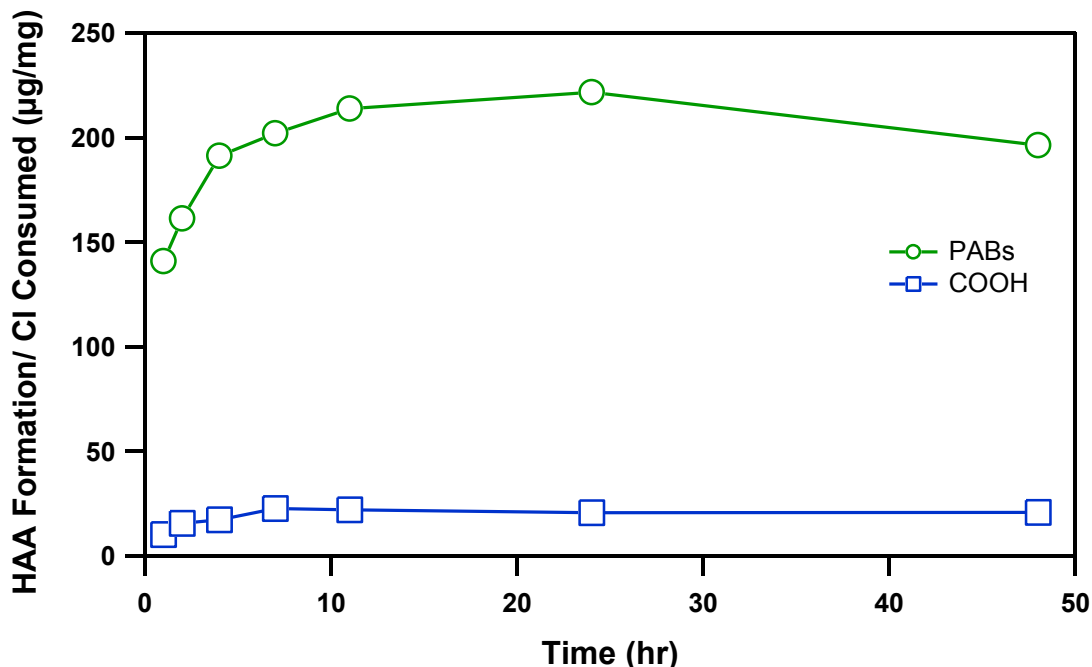


**Figure 3.8.** HAA formation per chlorine consumed as a function of time for CS PABS and CS SWCOOH.

### 3.5 Oxidation State of Carbon Nanotubes

Results thus far clearly show that the presence of surface oxide groups (e.g., surface carboxylic acid groups) promotes HAA formation. Indeed, as shown in Figure 3.9, there appears to be a reasonably strong correlation between total HAA formation and the concentration of surface oxygen on the CNT surface, regardless of the mechanism by which surface oxygen was added to the CNT surface (e.g., acid oxidation versus extended ozonation). The role of surface oxygen in DBP formation was studied by using XPS to measure the relative total surface oxygen concentrations of various CNTs, which is the O(1s) area in a survey scan with the background subtracted. Data are shown for all CNTs investigated. In addition to non-functionalized (as-received) CNTs, oxidized CNTs (via reflux with concentrated acids), and commercially available N-CNTs, we also include results from CT MWNF that were aged with aqueous ozone and germicidal UV.

Ozonation of suspended CNTs is an effective treatment to remove impurities while oxidizing the surface of with functional groups like carboxyl, carbonyl and hydroxyl on the surface of the CNT [54, 65, 66] to promote suspension stability. The likely rise in DBP formation is due to the formation of amorphous-like carbon particulates that have been identified after extensive ozonation in the gas phase [67]. This is similar to the cutting of CNTs and etching of the surface [68] during ozone exposure in the gas phase, which would cause an increase in reactive surface sites.

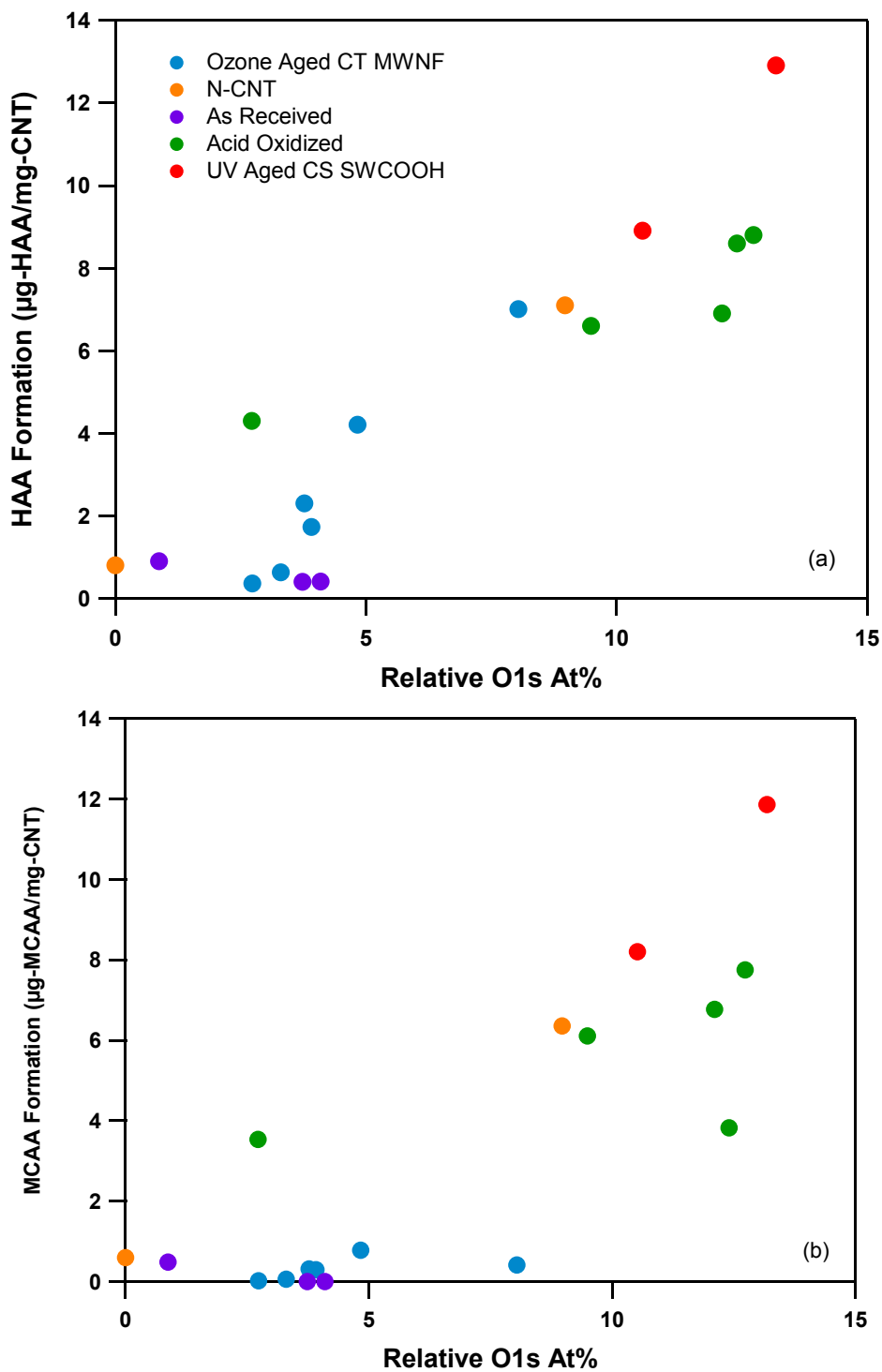
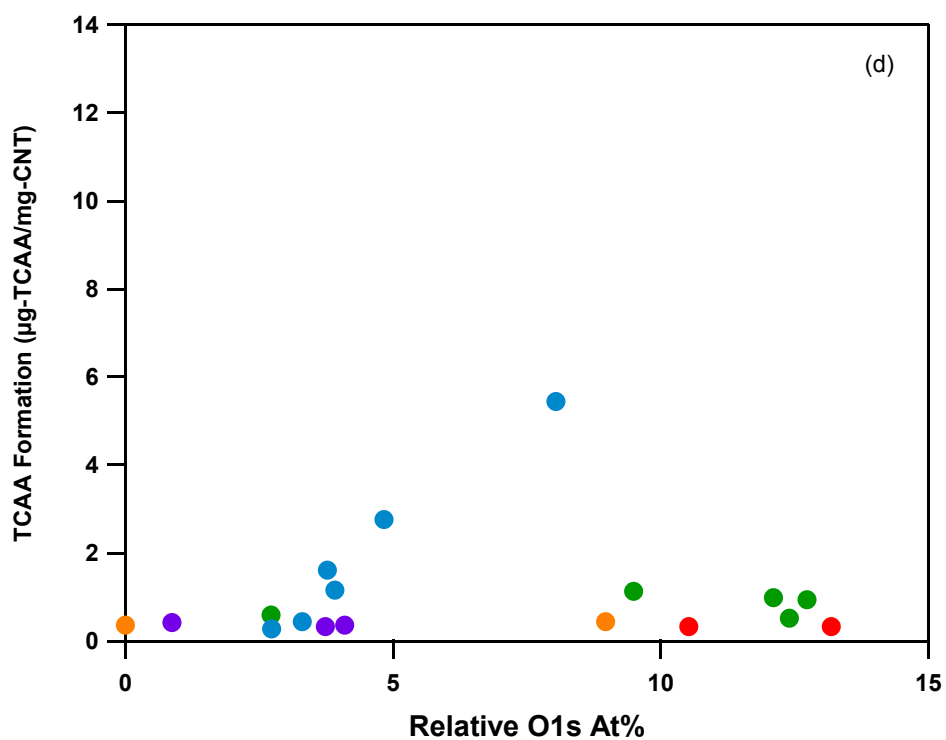
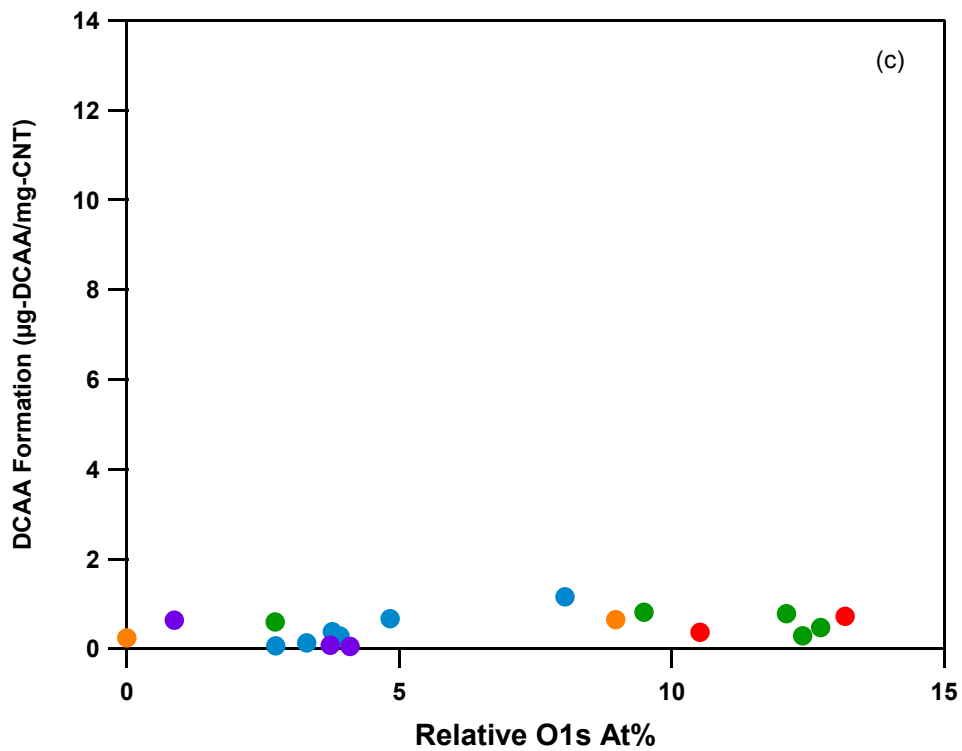
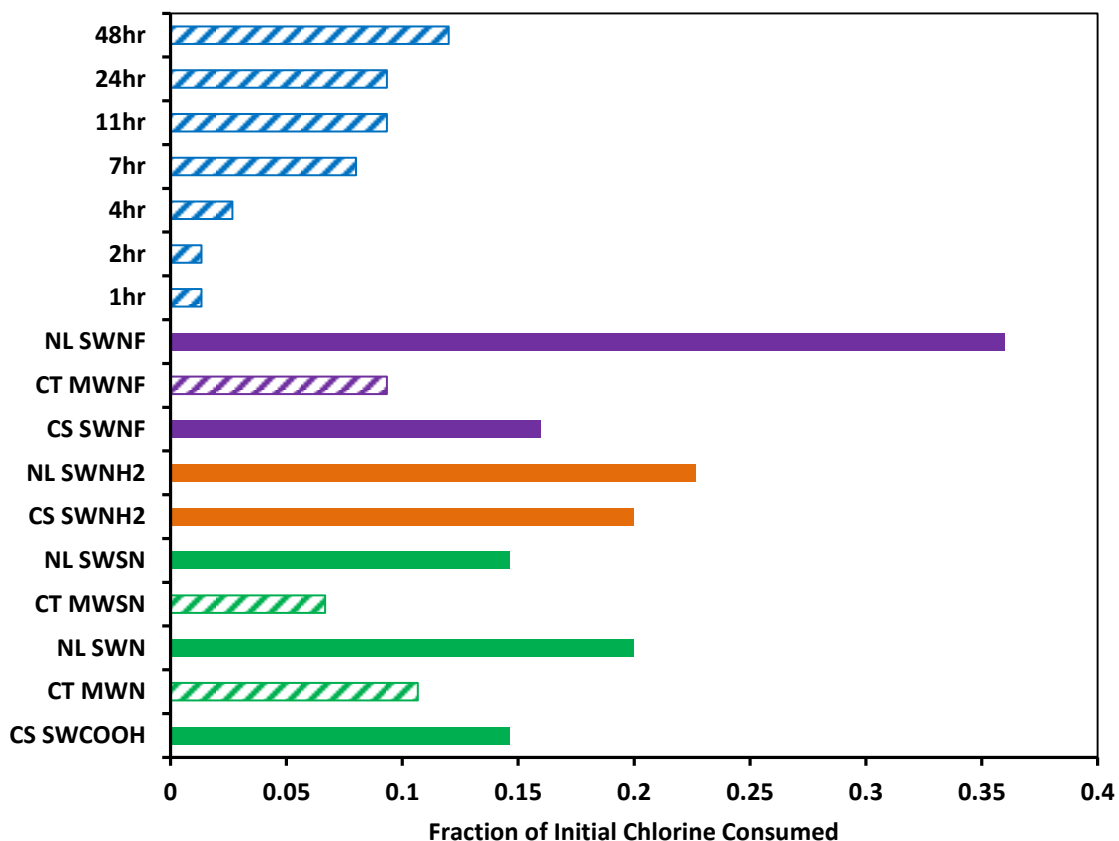


**Figure 3.9.** (a) Total HAA, (b) MCAA, (c) DCAA, and (d) TCAA formation per CNT loading as a function of surface oxygen content as measured by the O 1s region from XPS. All figures are on the same y-axis for comparison between different HAA classes.



Clearly, CNTs that exhibited greater surface oxygen concentration yielded the highest total haloacetic acid concentrations. However, while total HAA formation was

independent of the method of surface oxidation, the relative yield of individual HAAs was influenced by surface oxidation method. For example, while the acid oxidized CNTs contained the highest oxygen surface content and subsequently formed the most total HAAs, HAAs in these acid-oxidized CNT systems were dominated by MCAA formation. Interestingly, acid oxidized CNTs from NL contained the highest surface oxygen content but yielded the lowest amount of DCAA. Additionally, CNTs oxidized with nitric acid yielded the lowest amount of all HAAs as compared to other acid oxidized CNTs. Figure 3.9 confirms our thoughts on why the CS SWNH<sub>2</sub> produced HAA, while NL SWNH<sub>2</sub> did not. Surface oxygen content is nearly three times higher on CS SWNH<sub>2</sub>, and produces HAA in the same range of CNTs with similar surface oxygen content. This trend helps to better explain the previously reported difference between amine and amide functionalized CNTs. Ozone aged CT MWNF increased in oxygen content as aging increased, while also increasing in HAA yields. Unlike other CNTs, ozone aged CT MWNF HAA production was dominated by TCAA.



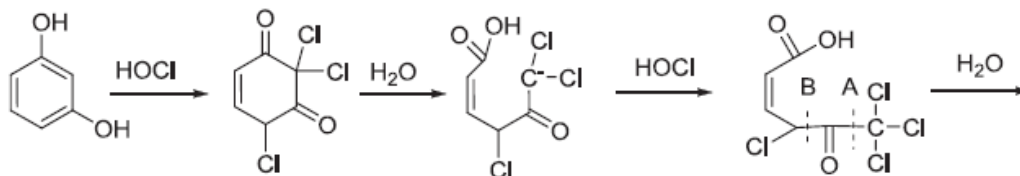
**Figure 3.10.** Fraction of initial chlorine consumed after reacted with chlorine for 4 h. Experiments were conducted in 5 mM phosphate buffer of 10 mg/L CNT loading and 15 mg/L HOCl dose.

Figure 3.10 shows the chlorine demand associated with each CNT after 4 h of reaction time with chlorine. Chlorine consumption of ozone aged CNTs increased with an increase in exposure to ozone (i.e., “aging time”). Furthermore, CT MWNF aged with O<sub>3</sub> for 48 h contained similar oxygen content and produced similar yields of HAA. Therefore, we believe that CNT sites that generate HAAs are not unique.

In a companion study, Verdugo [62] found that the manner in which the CNTs were oxidized strongly influenced chloroform formation. He identified that most surface oxidized (acid oxidized) and non-functionalized (as-received) CNTs resulted in little to

no appreciable chloroform formation. However, CNTs that were oxidized via extended ozonation produced a near linear increase in chloroform production with surface oxygen content. Interestingly, the same degree of surface oxygen on acid treated CNTs or CNTs aged via extended exposure to UV light did not produce similar amounts of chloroform upon chlorination. Thus, there appears to be something unique to the oxidation of CNTs with ozone that promotes their ability to generate chloroform, whereas the types of sites generating HAAs are not unique.

One particular trend of note is the correlation of TCAA and chloroform formation of the ozone aged CNTs. These CNTs are the only ones that show an increase in TCAA and chloroform yields with an increase in surface oxygen content. This is likely due to a similar surface intermediate in the ozone aged CNTs that have the ability to produce both TCAA and chloroform. The surface of these CNTs is similar to that of resorcinol. The mechanism for TCAA and chloroform formation via the chlorination of resorcinol is shown in Figure 3.11. Cleavage can occur at either A to yield chloroform, or at B to yield TCAA.



**Figure 3.11.** Mechanism of TCAA and chloroform formation via the chlorination of resorcinol.

### 3.6 Environmental Implications

The work accomplished in this study further verified that carbon nanotubes represent a source and precursor to disinfection byproducts. By identifying material

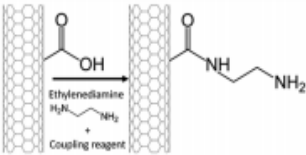
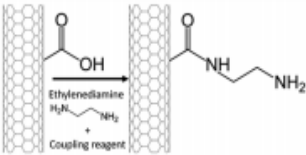
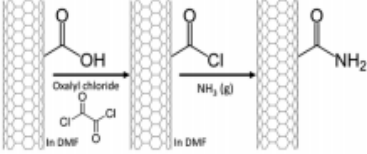
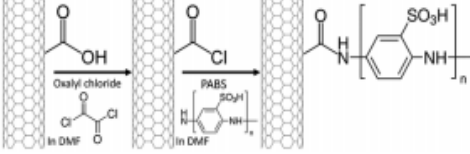
properties of CNTs, we are able to predict which CNTs promote reactivity toward chlorine-based disinfectants. CNT surface functional moieties play a large part in the extent of which DBPs are produced. The surface oxygen and surface oxidation routes are the primary contributors to haloacetic acid formation. Thus, CNT sites that generate HAAs are not unique as compared to trihalomethane formation. Results also show that CNTs behave similar to model precursors for di- and trichloroacetic acid formation. However, monochloroacetic acid is generated at significantly higher levels than found in most model precursors.

CHAPTER 4  
N-NITROSODIMETHYLAMINE PRODUCTION DURING THE CHLORINATION  
OF CARBON NANOTUBES

4.1 Introduction

Recently, Verdugo et al [61] investigated N-functionalized carbon nanotubes (N-CNTs) and discovered they are both a source and precursor for NDMA. As a source, NDMA was observed to leach from the surface of commercially available N-CNTs with amine, amide, or N-containing polymer (PABS) surface groups (see Table 4.1), presumably from the production of byproduct NDMA during the addition of N-containing surface groups to initially oxidized (i.e., carboxylated) CNTs.

**Table 4.1.** N-CNTs utilized in the Verdugo study.

Manufacturer	Name	Dimensions <sup>a</sup>	Surface area (m <sup>2</sup> /g) <sup>b</sup>	Surface Group and Vendor's Functionalization Route <sup>d</sup>
NanoLab	NL SWNH <sub>2</sub>	D = 1.5 nm avg L = 1-5 μm	860	
	NL MWNH <sub>2</sub>	OD = 15 nm avg L = 1-5 μm	250	
Carbon Solutions, Inc	CS SWNH <sub>2</sub>	D = 1.5 nm avg L = 0.5-3 μm	100 <sup>c</sup>	
	CS PABS	D = 1.5 nm avg L = 0.5-3 μm	6.5 <sup>c</sup>	

Upon dispersion of N-CNT powders, NDMA present on the surface of N-CNTs as a dried residue was solubilized, resulting in up to 50 ng of NDMA per mg of CNT in suspensions. Additionally, NDMA formation was investigated during the reaction of N-CNTs with chemical disinfectants including chlorine (HOCl), ozone, and

monochloramine. All N-CNTs were found to generate NDMA upon oxidation, with evidence supporting a surface reaction in which nitrogen on the CNT surface was incorporated into NDMA. In some cases, the yield of NDMA (in ng produced per mg of precursor) in these disinfectant systems was on par with those previously reported for natural organic matter (NOM) from surface water sources [69]. Evidence in support of surface-mediated route for NDMA production included evidence of CNT surface chlorination, as well as a decrease in surface N concentration, after N-CNT reaction. There was also an obvious increase in surface oxygen concentration.

Despite this evidence of a surface mediated route to NDMA production, mechanistic details of its formation during chlorination of N-CNT systems remain unclear. One outstanding question relates to the role of the CNT surface in NDMA production, specifically whether the electron rich sidewalls of the CNT are critical for NDMA production. For example, a notable observation from the work of Verdugo et al. was that solutions of ethylenediamine (EDA), which represent the nitrogen-containing precursor used for surface functionalization by NanoLabs, Inc. to produce amine-functionalized N-CNTs, failed to yield any NDMA across a range of EDA and free chlorine concentrations. The lack of NDMA production in these EDA solutions may imply a critical role for the CNT surface in NDMA formation. For example, EDA attachment to the CNT surface may produce a unique surface functional group that is not only reactive toward chlorine but also results in NDMA formation. Alternatively, the reaction of free chlorine with the CNT sidewall may produce highly reactive, short-lived intermediates necessary for NDMA production that must be in close proximity to

nitrogen to yield NDMA (as would be the case when EDA is tethered to the CNT surface).

Here, we attempt to better understand the formation of NDMA during chlorination of N-CNTs, exploring the role that surface association of EDA on different forms of CNTs plays in NDMA production. Using as-received (non-functionalized) CNTs, oxidized CNTs, and CNTs coated in the polymer PEG, we further examine if physical mixtures of CNTs and EDA can replicate the NDMA formation observed for NanoLabs, Inc. aminated N-CNTs. In addition to chlorination studies for quantifying NDMA yield as a function of several reagent parameters (e.g., CNT loading, EDA concentration, free chlorine concentration), we also conducted isotherm experiments examining the extent of EDA uptake on various CNTs in hopes of correlation observations of NDMA formation with the surface concentration of EDA resulting from sorption. Results from this study are consistent with a unique role for the CNT surface in NDMA formation, and suggest that there may be synergetic reactivity toward free chlorine resulting in NDMA formation for nitrogen-functionalized CNTs that cannot be readily predicted from the behavior of reagents used to develop N-CNTs.

#### 4.2 NDMA Formation via the Reaction of Carbon Nanotubes, Chlorine, and Ethylenediamine

The majority of experiments here utilized non-nitrogen containing CNTs, exploring whether their physical mixtures with EDA exhibit the ability to generate NDMA. These CNTs were introduced in Chapter 2 as either single-walled (SW) or multi-walled (MW) CNT varieties purchased from Carbon Solutions (CS), CheapTubes.com (CT) and NanoLabs, Inc. (NL). These included as received (non-

functionalized or NF) CNTs from CS (CS SWNF), NL (NL SWNF) and CT (CT MWNF). Two different forms of commercially available carboxylated (COOH) CNTs were considered from CS (CS SWCOOH) and NL (NL SWCOOH). Finally, we also considered one form of polymer coated CNT from CS modified with PEG (CS PEG). We also included the results observed from CS PABS as a representation of N-CNTs. For these CNTs, experiments as detailed in Chapter 2 explored their ability to generate NDMA both in the presence and absence of ethylenediamine (EDA up to 5000  $\mu\text{g/L}$  concentration) in the suspension (10 mg/L) of CNTs. Table 4.2 shows NDMA formation from initial experiments exploring NDMA formation when CNTs (10 mg/L) were reacted with 1000  $\mu\text{g/L}$  of EDA and 15 mg/L of HOCl. Control samples of either HOCl alone (without CNTs or EDA in suspension), mixtures of EDA and HOCl (without CNTs in suspension), and mixtures of CNTs and EDA (without HOCl) did not produce any NDMA.

**Table 4.2.** NDMA formation from commercial non N-CNTs and CS PABS at 10 mg/L when reacted with 15 mg/L HOCl and 1000  $\mu\text{g/L}$  EDA. \*CS PABS produced NDMA with and without the presence of EDA.

CNT	NDMA Formation (ng/L)
CS SWNF	ND
CS SWCOOH	ND
CS PEG	39.9
CS PABS*	36.8
CT MWNF	ND
NL SWNF	ND
NL SWCOOH	ND

As expected from the work of Verdugo et al., chlorination of CS PABS generated 36 ng/L of NDMA, which is within the range reported previously (50 $\pm$ 15 ng/L). Thus, the addition of EDA exerted no additional influence on NDMA formation in CS PABS,

which containing nitrogen in their surface polymer group that is likely integral to NDMA formation. Interestingly, CS PEG was the only non-nitrogen-containing CNT to produce NDMA during chlorination in the presence of EDA. All non-functionalized and oxidized CNTs were unable to combine with EDA to generate NDMA. Thus, additional studies were conducted to explore factors controlling NDMA formation in the CS PEG system, and how the fate of EDA in these systems may be different from those of other CNTs.

In CS PEG suspensions, chlorine decay and corresponding NDMA production from CS PEG are shown in Figure 4.1. Notably, the initial rate of NDMA formation is very fast, with ~20 ng/L of NDMA being produced in the first hour. This time interval also corresponds to a period with relatively large chlorine demand, where ~65% of the chlorine was consumed. After this initial period, the rate of NDMA formation slowed but was sustained, and chlorine continued to decay over the entire experimental period. After 24 h, 40 ng/L of NDMA had been produced while 95% of the initial chlorine had been consumed. The slowing rate of NDMA formation is consistent with a 2<sup>nd</sup> order reaction in which HOCl reacts with another species (either the CNT surface or the EDA in solution), and the rate of this reaction slows over time as HOCl is consumed.

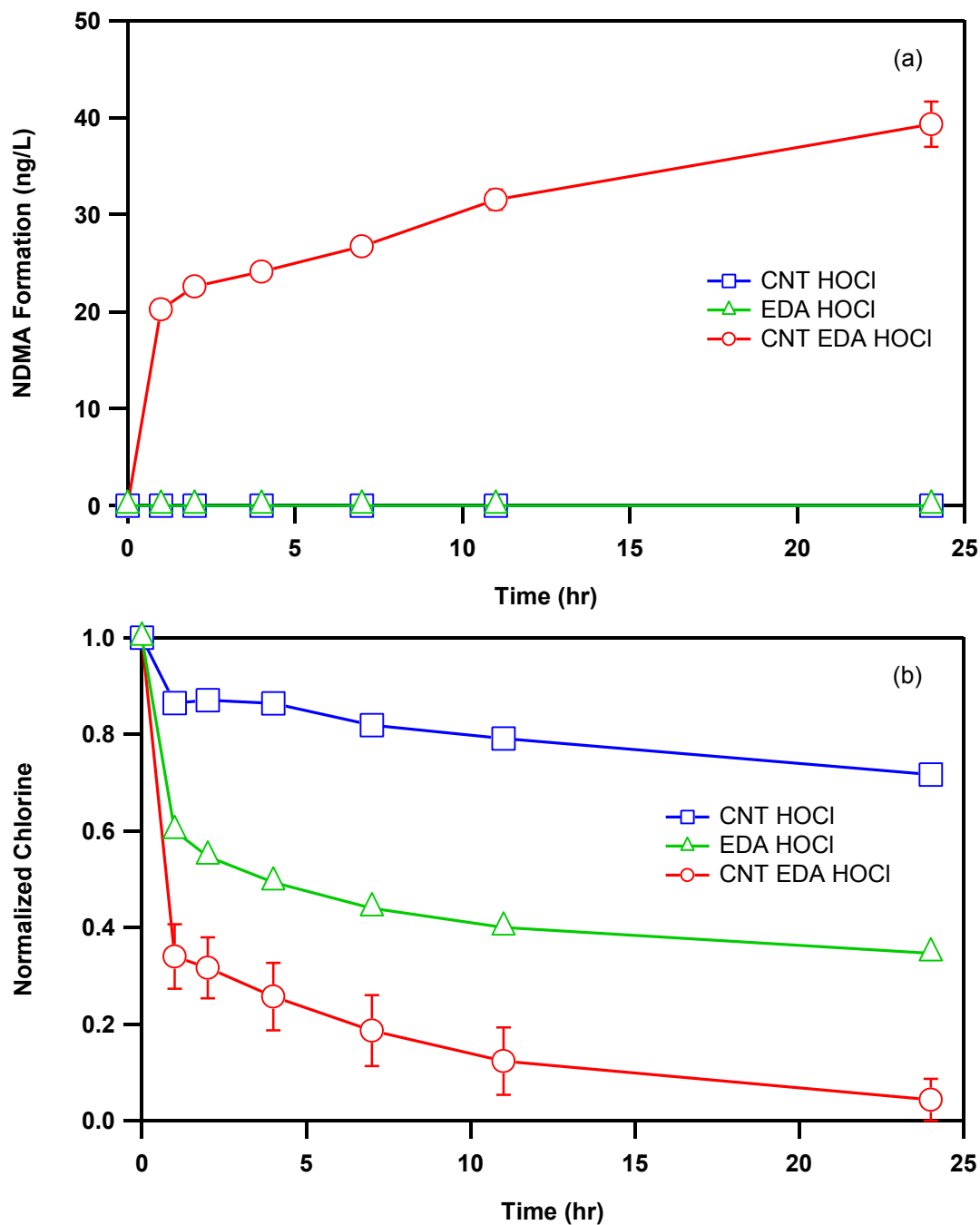


**Figure 4.1.** (a) NDMA formation and (b) normalized chlorine consumption during chlorination of CS PEG suspension. Experiments were conducted at pH 8 in 5 mM phosphate buffer with 10 mg/L CS PEG CNT loading, 15 mg/L HOCl, and 2000  $\mu$ g/L EDA.

As evident in Figure 4.1, the addition of EDA to CS PEG and HOCl greatly enhances chlorine demand. When comparing the chlorine consumption of EDA and

HOCl and the addition of CS PEG to this system, the CNT enhances chlorine consumption. This same trend is seen throughout the rest of this chapter, even when varying EDA concentrations. It seems that there is an additive effect with the addition of each component to the mixture. It is evident that both EDA and the CNT are active towards chlorine, and when combined the majority of the chlorine is consumed after 24 h. One reason EDA is so reactive is due to its ability to form chloramines with HOCl via the reaction at both of the N centers in EDA.

### 4.3 EDA Sorption

One scenario that could explain NDMA production in CS PEG systems is that EDA adsorbs to the PEGylated surface, thereby generate a surface analogous to CS PABs (i.e., with surface N available in the polymer) that may be optimal for NDMA production. Figure 4.2 shows the adsorption isotherm curve of EDA in CS PEG suspensions, where sorbed EDA concentration is plotted as a function of the concentration of EDA remaining in solution at equilibrium. Sorbed concentrations were determined by the difference in mass from the initial amount of EDA added to solution to the amount present in solution at equilibrium (24 h).

In CS PEG suspensions, sorption of EDA follows the expected shape for a Langmuir isotherm, where a near linear initial increase in sorbed concentration ultimately plateaus at a maximum sorbed concentration of  $\sim 100 \mu\text{g EDA/mg CNT}$  (corresponding to an equilibrium solution phase concentrations greater than  $3000 \mu\text{g/L}$ ). Notably, this maximum amount of sorbed EDA represents 40 percent of the total amount of EDA in the system (with the amount of sorbed EDA ranging from 2-40 percent). This has important implications for NDMA formation; increases in the sorbed concentration will

result in more N associated with the CNT surface, which may help to promote NDMA formation. Interestingly, from the chlorine demand data in Figure 4.1, this sorbed phase of EDA must remain reactive toward HOCl, as the chlorine demand in the mixture of EDA and CNTs is essentially the sum of the demand in each system independently. Meanwhile, the loss of EDA from solution is also beneficial, as it limits the reaction of dissolved NDMA with HOCl, which we know does not result in NDMA formation.

Additionally, we observed EDA uptake in NL SWCOOH and NL SWNF, similar to what we see in CS PEG. However, the surface N in this case does not promote NDMA formation in the mixture. This likely suggests a unique reaction sequence or entity in the CS PEG system necessary for NDMA formation. This may have to do with how the EDA sorbs to the CNT surface; in the PEG system it could be associated with the PEG primarily, while in the COOH and NF systems, it could be associated with the carbon on the CNT surface. This could influence the location of HOCl reaction in these systems (e.g. EDA on the CNT surface could block reactive sites), and in turn influence NDMA formation.

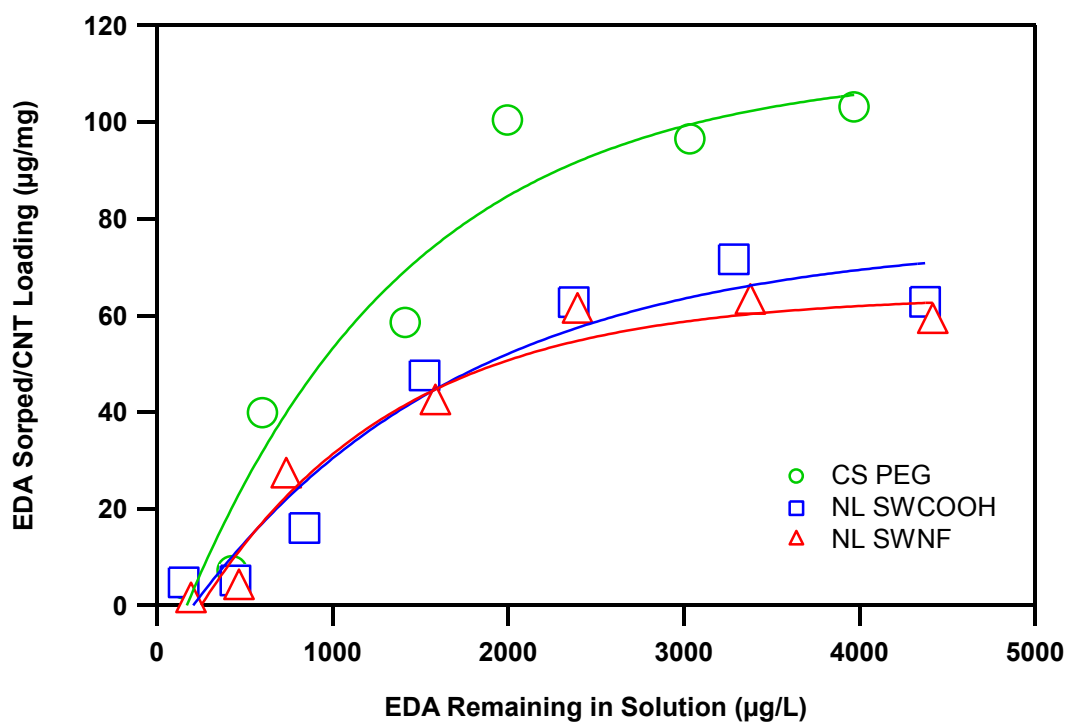


**Figure 4.2.** EDA sorption per CNT loading as a function of EDA remaining in solution. Experiments were conducted at pH 8 in 5 mM phosphate buffer with 10 mg/L of CS PEG, NL SWCOOH, and NL SWNF and reacted with varied EDA concentrations (200 - 5000 µg/L) for 1 day.

#### 4.4 Experimental Variables Influencing NDMA Formation in CS PEG Suspensions

Additional studies were conducted to understand the experimental factors most influential to NDMA formation in CS PEG suspensions containing EDA. Figure 4.3 shows the extent of chlorine decay (fractional removal from a 15 mg/L dose) and NDMA formation in 10 and 20 mg/L suspensions of CS PEG CNT. Data in Figure 4.3 were collected after 24 h of reaction, and are presented as a function of added EDA concentration, which was varied in these systems to explore its influence on available N.

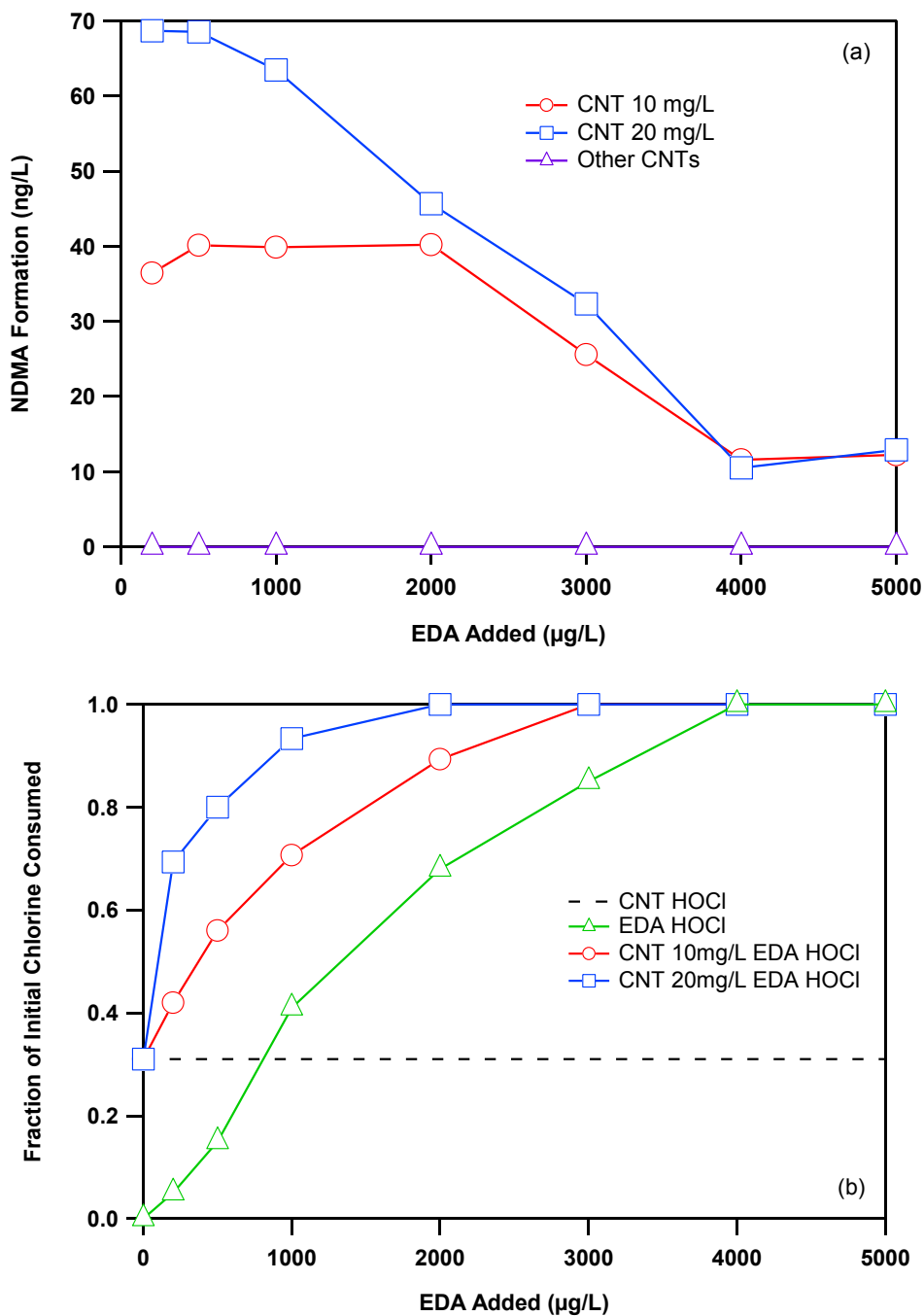


**Figure 4.3.** (a) NDMA formation and (b) fraction of initial chlorine consumed as a function of varied EDA added for varied CS PEG loadings. Experiments were conducted at pH 8 in 5 mM phosphate buffer with 15 mg/L of HOCl reacted for 1 day.

Figure 4.3 helps to explain the relationship between NDMA formation and chlorine demand in CS PEG and EDA mixtures. At relatively low EDA concentrations

(200 – 1000  $\mu\text{g/L}$ ), NDMA formation is roughly two-fold greater at the higher CS PEG concentration, as would be consistent for a surface chemical process that is limited by available reaction sites. The same dependence on CS PEG loading is observed for chlorine demand at 200  $\mu\text{g/L}$  of EDA, where suspensions of 20 mg/L of CS PEG consumed twice as much chlorine as the 10 mg/L suspensions (70% vs. 30 %, respectively). However, as the amount of EDA in the mixture is increased, both NDMA formation and chlorine demand begin to converge in 10 and 20 mg/L CS PEG suspensions. This is most clearly seen above 3000  $\mu\text{g/L}$  of EDA, when both suspensions are able to consume all available chlorine while producing near equivalent amounts of NDMA.

The results in Figure 4.3 seem to suggest competing reaction processes in CS PEG suspensions containing EDA, while suggesting that consumption of surface associated EDA is required for NDMA formation. A key observation is that EDA exerts a relative highly chlorine demand. Thus, any EDA that is not surface associated and dissolved in solution will compete with the CNT surface for available HOCl. Indeed, we believe this competition explains the trends in Figure 4.3. At low concentrations of added EDA, the relative small amount that remains in solution does not significantly contribute to HOCl consumption, allowing for a greater extent of HOCl with the CS PEG surface and any surface associated EDA. In contrast, as higher concentrations of EDA added, especially where the CNT surface saturates, the greater amount of soluble EDA results in a relatively large HOCl demand, which notably occurs without any NDMA formation. Thus, it is only at low EDA concentrations where sufficient HOCl reacts at the surface to produce the greatest extent of NDMA. The decrease in NDMA production at higher

EDA concentrations (at this initial value of 15 mg/L of HOCl) seems to suggest NDMA formation is limited not by available surface N (in the form of adsorbed EDA), but available HOCl.

#### 4.5 Effect of Chlorine Dose

To explore such a chlorine limitation, additional experiments examined NDMA production in CS PEG suspensions as a function of both EDA concentration and initial HOCl concentration. Figure 4.4 shows NDMA production across the same range of EDA concentrations, but also comparing the prior data for 10 mg/L CS PEG loadings with 15 mg/L of HOCl to results obtained at 5 and 30 mg/L initial HOCl concentrations. Consistent with HOCl being the limiting reagent in EDA and CS PEG mixtures, the lowest chlorine dose (5 mg/L) generated the lowest amount of NDMA. Once again, maximum NDMA production (~25 ng/L) occurred at the lowest EDA concentration explored (200 µg/L), while NDMA formation decreased and eventually became independent of added EDA at higher concentrations. Not surprisingly, the constant NDMA production observed 1000 µg/L coincides with conditions in which all available HOCl is consumed in these reactors.

Notably, NDMA production increased with increasing EDA at the higher chlorine dose of 30 mg/L, resulting in as much as 80 ng/L of NDMA at 4000 µg/L EDA. Not surprisingly, the increase in initial HOCl resulted in residual HOCl being measurable after 24 h at all but the highest EDA concentration considered. At this higher concentration of HOCl, therefore, the combination of increasing amounts of surface associated EDA (see Figure 4.2) along with available HOCl in suspension allows for sustained, and even increasing, NDMA production across the system variables explored.

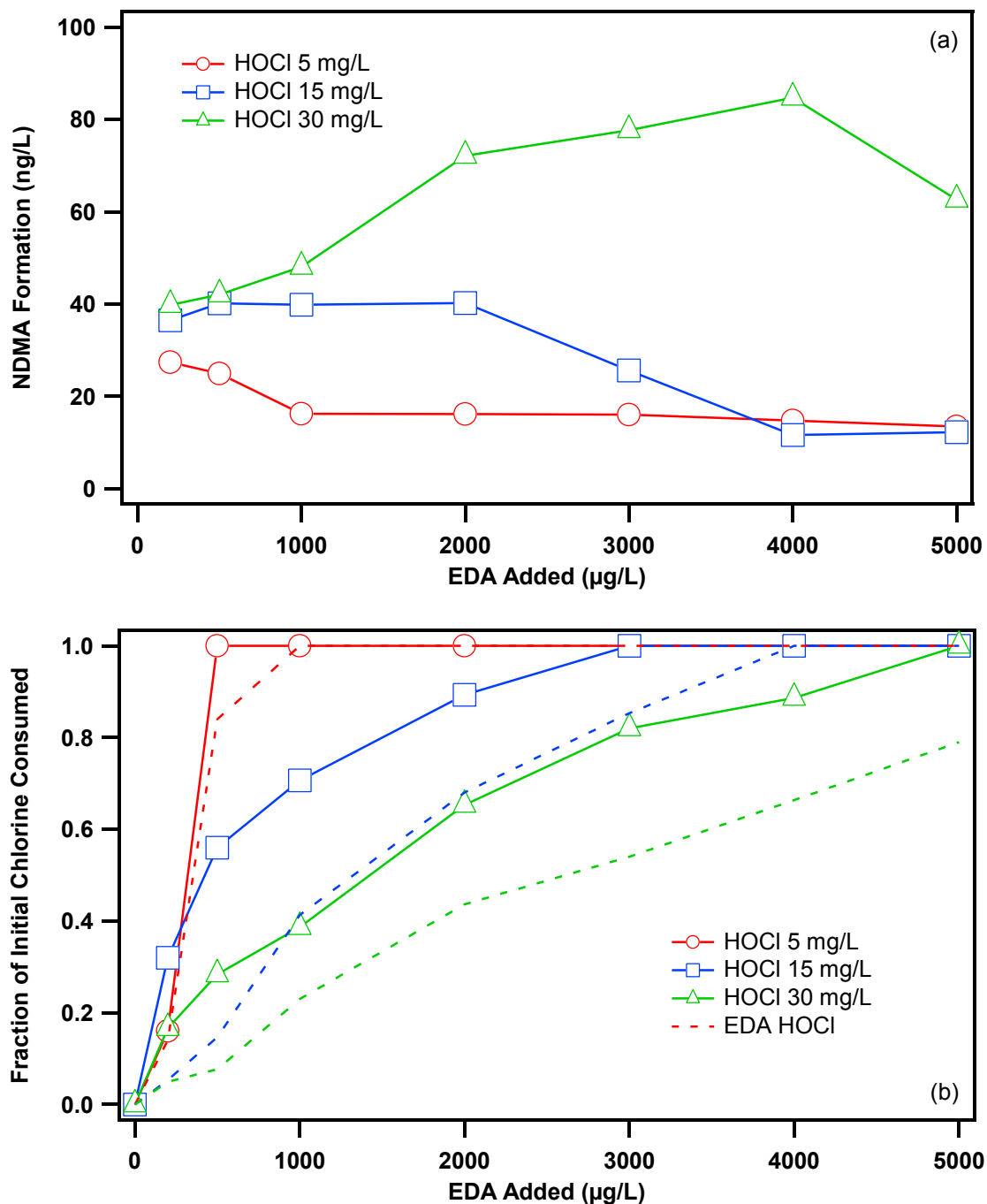


**Figure 4.4.** (a) NDMA formation and (b) fraction of initial chlorine consumed as a function of EDA added for varied HOCl doses. Experiments were conducted at pH 8 in 5 mM phosphate buffer with a fixed loading of CS PEG (10 mg/L) and reacted for 1 day.

#### 4.6 Conclusions

Ultimately, these experiments suggest that surface association of EDA is necessary for NDMA production in CNT suspensions, which we presume suggests that sorbed EDA is the source of N in NDMA production in these systems. Further, our data highlight a complex reaction pathway where surface and bulk solution reactions compete for HOCl, with only those surface mediated processes being able to generate NDMA. At lower EDA, when plenty of HOCl is available in the solution, NDMA formation appears most likely limited by the amount of EDA that is surface associated through sorption. In contrast, at higher EDA concentrations, EDA remains free in solution (rather than adsorbed) where it can also exert a chlorine demand, competition between freely dissolved EDA and the CNT surface for HOCl works to limit NDMA formation.

While the mechanism of NDMA formation is clearly surface mediated, the exact steps in the reaction sequence are not yet clear. Nor is it well understood why surface associated EDA on other forms of CNTs (e.g., CS SWNF and CS SWCOOH, see Figure 4.3) do not result in NDMA formation when EDA linked to carboxylated CNTs were previously shown to yield NDMA during chlorination. We can only conclude that EDA physisorbed on the CS SWCOOH results in differences in the chemical reactivity of the surface associated N relative to EDA that is chemically linked to the –COOH surface moiety via chemical reaction.

We speculate that the similar degree of EDA uptake on CS SWNF and CS SWCOOH suggests that EDA sorption does not proceed through interactions with surface –COOH groups (which will be deprotonated at the pH used in our systems), but rather via interactions occurring primarily on non-oxidized sites on the CNT surface.

The findings in these model systems can be extended to real world – specifically the role of available free and combined chlorine and its ability to control NDMA formation from CNTs. However, given the highly reactive site on N-CNTs, and that chlorine will always be “in excess” relative to trace levels of CNTs in wastewater, we can assume that CNTs will contribute to some level of NDMA production if entered into a water or wastewater treatment facility.

## CHAPTER 5 ENVIRONMENTAL IMPLICATIONS AND FUTURE WORK

### 5.1 Environmental Implications

The work accomplished in this study further verified that carbon nanotubes (CNTs) represent a source and precursor to disinfection byproducts (DBPs). By identifying material properties of CNTs, we are able to predict which CNTs promote reactivity toward chlorine-based disinfectants. CNT surface functional moieties play a large part in the extent of which DBPs are produced. The surface oxygen and surface oxidation routes are the primary contributors to haloacetic acid (HAA) formation. Thus, CNT sites that generate HAAs are not unique with respect to trihalomethane (THM) formation. Results also show that CNTs behave similar to model precursors for di- and trichloroacetic acid formation (DCAA and TCAA, respectively). However, monochloroacetic acid (MCAA) is generated at significantly higher levels than found in most model precursors.

Nitrogen containing CNTs have been shown as source of N-nitrosodimethylamine (NDMA). Surprisingly, CS PEG, which does not contain N, produces NDMA when reacted in the presence of chlorine (HOCl) and ethylenediamine (EDA). Ultimately, EDA is contributing N to CS PEG by sorbing to the CNT surface, which is the likely source of N for NDMA formation. At lower EDA concentrations, NDMA production is limited by available EDA. Conversely, at higher EDA concentrations, NDMA production is limited by available chlorine that is in competition with EDA and the CNT surface. Furthermore, it is evident that CNT surface and solution chemistry is important to determine the formation potential of NDMA in this system.

Our work illustrates how functionalized CNTs can mimic the reactivity of natural organic matter (NOM). This will improve the ability of engineers and scientists to predict the fate and effects of CNTs in the environment. We can assume that free and combined chlorine will always be in excess in wastewater and water treatment systems, therefore allowing us to understand the extent at which DBPs can form if CNTs enter the system. Thus, we can assess the impact of CNT cytotoxicity on aquatic species. This work highlights the need to examine emerging pollutants such as engineered nanomaterials and their fate and transport in the environment. Hazardous byproducts that are potentially carcinogenic have the ability to enter our drinking water.

### 5.2 Future Work

There are still several other emerging DBP classes to examine as potential hazardous byproducts of chlorination of CNTs. Future studies should involve using more complex aquatic matrices to establish the influence of aquatic chemical variables on the reactivity of CNTs toward disinfectants. Efforts can be focused on the influence of the addition of bromide and iodide. These two oxidants have been shown to generate brominated and iodinated byproducts in model precursors and NOM. Additionally, we can examine the influence of dissolved organic matter on CNT reactivity toward disinfectants. Many forms of organic matter are demonstrated precursors for DBP formation, and CNTs have the ability to concentrate organic matter on their surfaces via sorption. Thus, we can explore the rates and product distributions for the reaction of disinfectants with organic matter-coated CNT surfaces.

## REFERENCES

1. Deborde, M. and U. von Gunten, *Reactions of chlorine with inorganic and organic compounds during water treatment—Kinetics and mechanisms: A critical review*. Water Research, 2008. **42**(1–2): p. 13-51.
2. Davis, M.L., *Water and wastewater engineering : design principles and practice*. 2011, New York: McGraw-Hill.
3. Morris, J.C. and B. Baum, *Precursors and mechanisms of haloform formation in the chlorination of water supplies*. Water chlorination: environmental impact and health effects, 1978. **2**.
4. Dore, M., *Chimie des oxydants et traitement des eaux. Technique et Documentation Editeur, Paris*. 1989, ISBN 2-85206-562-2.
5. Esplugas, S., et al., *Comparison of different advanced oxidation processes for phenol degradation*. Water Research, 2002. **36**(4): p. 1034-1042.
6. von Gunten, U., *Ozonation of drinking water: Part I. Oxidation kinetics and product formation*. Water Research, 2003. **37**(7): p. 1443-1467.
7. Madigan, M., et al., *Brock Biology of Microorganisms (13th Edition)*. 2010: Benjamin Cummings.
8. Severin, B.F., M.T. Suidan, and R.S. Engelbrecht, *Kinetic modeling of U.V. disinfection of water*. Water Research, 1983. **17**(11): p. 1669-1678.
9. Radiant, U. *How does Ultraviolet sterilization work?* ; Available from: <http://www.radiantuv.com/uv-edu/>.
10. Kumar, K., R.A. Day, and D.W. Margerum, *Atom-transfer redox kinetics: General-acid-assisted oxidation of iodide by chloramines and hypochlorite*. Inorganic Chemistry, 1986. **25**(24): p. 4344-4350.
11. Gallard, H., A. Leclercq, and J.-P. Croué, *Chlorination of bisphenol A: kinetics and by-products formation*. Chemosphere, 2004. **56**(5): p. 465-473.
12. Pinkston, K.E. and D.L. Sedlak, *Transformation of aromatic ether- and amine-containing pharmaceuticals during chlorine disinfection*. Environmental Science and Technology, 2004. **38**(14): p. 4019-4025.
13. Richardson, S.D., et al., *Occurrence, genotoxicity, and carcinogenicity of regulated and emerging disinfection by-products in drinking water: A review and roadmap for research*. Mutation Research/Reviews in Mutation Research, 2007. **636**(1–3): p. 178-242.
14. Krasner, S.W., et al., *The occurrence of disinfection by-products in US drinking water*. Journal-American Water Works Association, 1989. **81**(8): p. 41-53.
15. Krasner, S.W., et al., *Occurrence of a New Generation of Disinfection Byproducts†*. Environmental Science & Technology, 2006. **40**(23): p. 7175-7185.
16. USEPA, *Basic Information about Disinfection Byproducts in Drinking Water: Total Trihalomethanes, Haloacetic Acids, Bromate, and Chlorite*. 2013: <http://water.epa.gov/drink/contaminants/basicinformation/disinfectionbyproducts.cfm#What> disinfection byproducts does EPA regulate, how are they formed, and what are their health effects in drinking water at levels above the maximum contaminant level?
17. USEPA, *Technical Fact Sheet – N-Nitroso-dimethylamine (NDMA)*. 2012: [http://www.epa.gov/fedfac/pdf/technical\\_fact\\_sheet\\_ndma.pdf](http://www.epa.gov/fedfac/pdf/technical_fact_sheet_ndma.pdf).

18. Mitch, W.A., et al., *N-nitrosodimethylamine (NDMA) as a drinking water contaminant: A review*. Environ. Eng. Sci., 2003. **20**(5): p. 389-404.
19. Plewa, M.J., et al., *Mammalian cell cytotoxicity and genotoxicity analysis of drinking water disinfection by-products*. Environ. Mol. Mutagen., 2002. **40**(2): p. 134-142.
20. Plewa, M.J., et al., *Mammalian Cell Cytotoxicity and Genotoxicity of the Haloacetic Acids, A Major Class of Drinking Water Disinfection By-Products*. Environ. Mol. Mutagen., 2010. **51**(8-9): p. 871-878.
21. Croue, J.-P., G.V. Korshin, and M.M. Benjamin, *Characterization of natural organic matter in drinking water*. 2000: American Water Works Association.
22. Kanokkantapong, V., et al., *FTIR evaluation of functional groups involved in the formation of haloacetic acids during the chlorination of raw water*. Journal of Hazardous Materials, 2006. **136**(2): p. 188-196.
23. Krasner, S.W. and G. Amy, *Jar-test evaluations of enhanced coagulation*. Journal-American Water Works Association, 1995. **87**(10): p. 93-107.
24. Liang, L. and P.C. Singer, *Factors Influencing the Formation and Relative Distribution of Haloacetic Acids and Trihalomethanes in Drinking Water*. Environmental Science & Technology, 2003. **37**(13): p. 2920-2928.
25. Reckhow, D.A., P.C. Singer, and R.L. Malcolm, *Chlorination of humic materials: byproduct formation and chemical interpretations*. Environmental Science & Technology, 1990. **24**(11): p. 1655-1664.
26. Kanokkantapong, V., et al., *Characterization of haloacetic acid precursors in source water*. Journal of Environmental Management, 2006. **80**(3): p. 214-221.
27. Hua, G. and D.A. Reckhow, *Characterization of Disinfection Byproduct Precursors Based on Hydrophobicity and Molecular Size*. Environmental Science & Technology, 2007. **41**(9): p. 3309-3315.
28. Chang, E.E., et al., *Relationship between chlorine consumption and chlorination by-products formation for model compounds*. Chemosphere, 2006. **64**(7): p. 1196-1203.
29. Trussell, R.R. and M.D. Umphres, *The formation of trihalomethanes*. American Water Works Association Journal, 1978. **70**(11): p. 604-12.
30. Peters, C.J., R.J. Young, and R. Perry, *Factors influencing the formation of haloforms in the chlorination of humic materials*. Environmental Science & Technology, 1980. **14**(11): p. 1391-1395.
31. Gallard, H. and U. von Gunten, *Chlorination of natural organic matter: kinetics of chlorination and of THM formation*. Water Research, 2002. **36**(1): p. 65-74.
32. Dickenson, E.R.V., et al., *Haloacetic acid and Trihalomethane Formation from the Chlorination and Bromination of Aliphatic  $\beta$ -Dicarbonyl Acid Model Compounds*. Environmental Science & Technology, 2008. **42**(9): p. 3226-3233.
33. Hong, H.C., M.H. Wong, and Y. Liang, *Amino Acids as Precursors of Trihalomethane and Haloacetic Acid Formation During Chlorination*. Archives of Environmental Contamination and Toxicology, 2009. **56**(4): p. 638-645.
34. Peters, R.J.B., E.W.B. De Leer, and L. De Galan, *Chlorination of cyanoethanoic acid in aqueous medium*. Environmental Science & Technology, 1990. **24**(1): p. 81-86.

35. Trehy, M.L., R.A. Yost, and C.J. Miles, *Chlorination byproducts of amino acids in natural waters*. Environmental science & technology, 1986. **20**(11): p. 1117-1122.
36. Bond, T., et al., *Chemical and biological oxidation of NOM surrogates and effect on HAA formation*. Water Research, 2009. **43**(10): p. 2615-2622.
37. Sharma, V.K., *Kinetics and mechanism of formation and destruction of N-nitrosodimethylamine in water – A review*. Sep. Purif. Technol., 2012. **88**(0): p. 1-10.
38. Padhye, L., et al., *PolyDADMAC and dimethylamine as precursors of N-nitrosodimethylamine during ozonation: reaction kinetics and mechanisms*. Environmental science & technology, 2011. **45**(10): p. 4353-4359.
39. Richardson, S.D. and C. Postigo, *Drinking water disinfection by-products, in Emerging organic contaminants and human health*. 2012, Springer. p. 93-137.
40. Wang, P., Y.-L. He, and C.-H. Huang, *Reactions of tetracycline antibiotics with chlorine dioxide and free chlorine*. water research, 2011. **45**(4): p. 1838-1846.
41. Dodd, M.C. and C.-H. Huang, *Transformation of the antibacterial agent sulfamethoxazole in reactions with chlorine: kinetics, mechanisms, and pathways*. Environmental science & technology, 2004. **38**(21): p. 5607-5615.
42. Shah, A.D., J.-H. Kim, and C.-H. Huang, *Reaction kinetics and transformation of carbadox and structurally related compounds with aqueous chlorine*. Environmental science & technology, 2006. **40**(23): p. 7228-7235.
43. McDowell, D.C., et al., *Ozonation of carbamazepine in drinking water: identification and kinetic study of major oxidation products*. Environmental science & technology, 2005. **39**(20): p. 8014-8022.
44. Nakajima, M., et al., *Aquatic fate of sunscreen agents octyl-4-methoxycinnamate and octyl-4-dimethylaminobenzoate in model swimming pools and the mutagenic assays of their chlorination byproducts*. J Health Sci, 2009. **55**(3): p. 363-372.
45. Kuhlich, P., et al., *Transformations of polycyclic musks AHTN and HHCB upon disinfection with hypochlorite: two new chlorinated disinfection by-products (CDBP) of AHTN and a possible source for HHCB-lactone*. Analytical and bioanalytical chemistry, 2011. **399**(10): p. 3579-3588.
46. Peng, X., et al., *Adsorption of 1, 2-dichlorobenzene from water to carbon nanotubes*. Chemical Physics Letters, 2003. **376**(1): p. 154-158.
47. Pan, B. and B. Xing, *Adsorption mechanisms of organic chemicals on carbon nanotubes*. Environmental Science & Technology, 2008. **42**(24): p. 9005-9013.
48. Voudrias, E.A., R.A. Larson, and V.L. Snoeyink, *Effects of Activated Carbon on the Reactions of Combined Chlorine with Phenols*. Water Res., 1985. **19**(7): p. 909-915.
49. Padhye, L.P., et al., *N-Nitrosamines Formation from Secondary Amines by Nitrogen Fixation on the Surface of Activated Carbon*. Environ. Sci. Technol., 2011. **45**(19): p. 8368-8376.
50. Mauter, M.S. and M. Elimelech, *Environmental applications of carbon-based nanomaterials*. Environmental Science & Technology, 2008. **42**(16): p. 5843-5859.
51. Hirsch, A. and O. Vostrowsky, *Functionalization of carbon nanotubes, in Functional molecular nanostructures*. 2005, Springer. p. 193-237.

52. Dresselhaus, M.S. and M. Endo, *Relation of carbon nanotubes to other carbon materials*, in *Carbon nanotubes*. 2001, Springer. p. 11-28.
53. Barone, V., et al., *Screened exchange hybrid density-functional study of the work function of pristine and doped single-walled carbon nanotubes*. *The Journal of chemical physics*, 2006. **124**(2): p. 024709.
54. Wepasnick, K.A., et al., *Surface and structural characterization of multi-walled carbon nanotubes following different oxidative treatments*. *Carbon*, 2011. **49**(1): p. 24-36.
55. Oulton, R.L., *Development of nanomaterial-enabled advanced oxidation techniques for treatment of organic micropollutants.*, in *Civil and Environmental Engineering*. 2013, University of Iowa.
56. Smith, B., et al., *Influence of surface oxides on the colloidal stability of multi-walled carbon nanotubes: A structure– property relationship*. *Langmuir*, 2009. **25**(17): p. 9767-9776.
57. Zhao, B., et al., *Synthesis and characterization of water soluble single-walled carbon nanotube graft copolymers*. *Journal of the American Chemical Society*, 2005. **127**(22): p. 8197-8203.
58. Clesceri, L.S., et al., *Standard Methods for the Examination of Water and Wastewater*. 1998: American Public Health Association.
59. Xie, Y., *Analyzing Haloacetic Acids Using Gas Chromatography/Mass Spectrometry*. *Water Research*, 2001. **35**(6): p. 1599-1602.
60. Dai, N. and W.A. Mitch, *Effects of Flue Gas Compositions on Nitrosamine and Nitramine Formation in Postcombustion CO<sub>2</sub> Capture Systems*. *Environmental Science & Technology*, 2014. **48**(13): p. 7519-7526.
61. Verdugo, E.M., et al., *N-Functionalized Carbon Nanotubes As a Source and Precursor of N-Nitrosodimethylamine: Implications for Environmental Fate, Transport, and Toxicity*. *Environmental science & technology*, 2014. **48**(16): p. 9279-9287.
62. Verdugo, E., *Civil and Environmental Engineering Department, University of Iowa, Iowa City, IA*. March 2015.
63. Chang, H., C. Chen, and G. Wang, *Identification of potential nitrogenous organic precursors for C-, N-DBPs and characterization of their DBPs formation*. *Water research*, 2011. **45**(12): p. 3753-3764.
64. Bond, T., et al., *Disinfection byproduct formation and fractionation behavior of natural organic matter surrogates*. *Environmental science & technology*, 2009. **43**(15): p. 5982-5989.
65. Morales-Lara, F., et al., *Functionalization of Multiwall Carbon Nanotubes by Ozone at Basic pH. Comparison with Oxygen Plasma and Ozone in Gas Phase*. *The Journal of Physical Chemistry C*, 2013. **117**(22): p. 11647-11655.
66. Vennerberg, D.C., et al., *Oxidation Behavior of Multiwalled Carbon Nanotubes Fluidized with Ozone*. *ACS Applied Materials & Interfaces*, 2014. **6**(3): p. 1835-1842.
67. Bekyarova, E., et al., *Chemically Engineered Single-Walled Carbon Nanotube Materials for the Electronic Detection of Hydrogen Chloride*. *Advanced Materials*, 2010. **22**(7): p. 848-852.

68. Chen, Z., et al., *Cutting of Single-Walled Carbon Nanotubes by Ozonolysis*. The Journal of Physical Chemistry B, 2006. **110**(24): p. 11624-11627.
69. Chen, Z. and R.L. Valentine, *Modeling the formation of N-nitrosodimethylamine (NDMA) from the reaction of natural organic matter (NOM) with monochloramine*. Environmental science & technology, 2006. **40**(23): p. 7290-7297.